Journal of Hydrology 580 (2020) 124246

Contents lists available at ScienceDirect

Journal of Hydrology

journal homepage: www.elsevier.com/locate/jhydrol

Research papers

Regional water-energy cycle response to land use/cover change in the agro-pastoral ecotone, Northwest China

Xuejin Wang[a], Baoqing Zhang[a,*], Xuefeng Xu[a], Jie Tian[a], Chansheng He[a,b,*]

[a] Key Laboratory of West China's Environmental System (Ministry of Education), College of Earth and Environmental Sciences, Lanzhou University, Lanzhou, Gansu 730000, China

[b] Department of Geography, Western Michigan University, Kalamazoo, MI 49008, USA

ARTICLE INFO

Keywords:
Land use/cover change
Land surface temperature
Evapotranspiration
Precipitation
Land-atmosphere interaction

ABSTRACT

A better understanding of responses of the regional water-energy cycle to land use/cover change (LUCC) is important for ecological restoration in the agro-pastoral ecotone, Northwest China (APENWC). In this study, we examined the responses to various types of LUCC in the APENWC during the implementation of the Grain-for-Green project between 1993 and 2010 using the weather research and forecasting (WRF) model. The performance of the WRF model was validated by multiple types of observations. Results show that the WRF can accurately simulate regional water and energy processes in the APENWC, and that the water-energy cycles in the region are strongly affected by vegetation dynamics. During the period of 1993 and 2010, the most obviously increased land cover types were the grassland and barren land, and the decreased land cover types were shrublands and croplands in the study region. A significantly negative correlation ($R^2 = 0.78$) between land surface temperature (LST) and albedo was found, associated with a 0.5 °C reduction in the annual mean surface temperature in the APENWC between 1993 and 2010. Negative correlations between changes in evapotranspiration (ET) and albedo during the period in all seasons were also detected, except summer, when the correlation was positive ($R^2 = 0.49$). This is attributed to transpiration from plants being the main contributor to ET in summer and, hence total ET. The changes resulted in an increase of ET by 19.79 mm in summer, and decreases of ET by 1.15 mm, 13.22 mm, and 0.96 mm, respectively, in spring, fall, and winter. The LUCC also resulted in reductions in precipitation (of 2.3, 7.31, and 7.8 mm in spring, summer, and fall, respectively) by altering local ET and vapor flux cycles in the APENWC, and the study region contributed additional moisture from the local ET into the north of the region. The findings show that the grassland expansion reduces mean land surface temperature, which will delay germination of seeds and initiation of vegetation growth in spring. Increases in seasonal ET and reductions in seasonal precipitation will lead to soil drying, exacerbating risks of summer drought in the APENWC. The findings provide important information in facilitating formulation of effective strategies for sustainable development and ecological restoration in the APENWC and similar regions.

1. Introduction

Human activities have drastically changed the Earth's surface and climate over the past few decades (Hossain et al., 2015; Pielke et al., 2016). Land Use/Cover Change (LUCC) has become a focal point of global change (Roy and Avissar, 2002; Foley, 2005, Rigden and Li, 2017). Studies have demonstrated that LUCC is a main driver of regional climate change (Bounoua et al., 2002; Pielke et al., 2011), it can directly alter land surface properties such as surface albedo, ground roughness, soil heat, and moisture, which have important effects on surface water-energy exchange processes (Pitman et al., 2009; Mahmood et al., 2010; Pielke et al., 2011). LUCC induced by human activities, such as deforestation or afforestation, land reclamation, and urbanization, have direct effects on surface hydrological processes (Bai et al., 2018; Legesse et al., 2003; Lejeune et al., 2014; Mao and Cherkauer, 2009; Mohan and Kandya, 2015; Wijesekara et al., 2012) and land-atmosphere interaction (Huang and Margulis, 2010; Pielke et al., 2011). Studies have indicated that surface vegetation change significantly affects the surface hydrological processes and water-energy cycle (Zhang et al., 2014; Zhang et al., 2016a; Zhang et al., 2016b; Cheng et al., 2017). For example, Qiao et al. (2017) found that woody plant encroachment reduces annual runoff and shifts runoff

* Corresponding authors at: Key Laboratory of West China's Environmental System (Ministry of Education), College of Earth and Environmental Sciences, Lanzhou University, Lanzhou, Gansu 730000, China.

E-mail addresses: baoqzhang@lzu.edu.cn (B. Zhang), he@wmich.edu (C. He).

https://doi.org/10.1016/j.jhydrol.2019.124246

Available online 21 October 2019

mechanisms. Deforestation increases catchment erosion and nutrient, annual discharges and surface runoff (Woodward et al., 2014; Guzha et al., 2018). These studies indicate that the impacts of LUCC vary over space and different climate and environmental conditions.

LUCC alters water and energy exchanges between the atmosphere and land surface, and strongly influences weather and climate over local and regional scales (Orlowsky and Seneviratne, 2010; Zabel et al., 2011; Harding et al., 2013; Zhang et al., 2013; Gao and Wu, 2014; Zhang et al., 2015; Boone et al., 2016). One of the most important surface parameters is albedo, the ability of land surface to reflect solar radiation. This is a major determinant of energy fluxes at the land surface, and its changes can significantly change land surface temperature and regional energy balance (Liu et al., 2014; Mohan and Kandya, 2015; Qu et al., 2013). Land surface temperature (LST) is a key parameter for radiation and heat fluxes at the land surface-atmosphere interface, which are largely controlled by the difference between the LST and near-surface air temperature (Liu et al., 2016a), its effects have been extensively studied in relation to weather forecasting, climate change, hydrological cycles, and agricultural processes (Deng et al., 2018; Zhang and Liang, 2018). Changes in LST have clear effects on regional ET (Dias et al., 2015), and ET, in turn, significantly influences soil moisture conditions by changing the surface energy distribution (Zhao et al., 2008). As a major component of both hydrological cycles and the surface energy balance, ET has also been affected in recent years by anthropogenic LUCC and climate change (Li et al., 2017). As an important source of precipitation in hydrological cycles, changes in ET and vapor flux transportation also significantly affect local precipitation patterns (Hagos et al., 2014; Wang et al., 2016; Xue et al., 2010). Since LST, ET and precipitation are all extremely sensitive to LUCC (Li et al., 2017; Wang et al., 2015b), assessment of LUCC's effects on these factors is crucial for deep understanding of surface water and energy exchange processes.

Precipitation is an important resource for maintaining the sustainable development of agriculture and other related socio-economic activities in the agro-pastoral ecotone, Northwest China (APENWC). Generally, there are two sources of precipitation in a region: (1) water vapor evaporated within the region, and (2) water vapor transported into the region from outside (Brubaker et al., 1993). The response of precipitation to LUCC is a higher percentage of the precipitation from the water vapor evaporated within the region, Zhao et al. (2016) and Wei et al. (2012) indicated that the local water cycles have most contribution to the precipitation over Northwest China. The relationships between local ET, precipitable water and precipitation recycling may be good indicators of regional hydrological variations (Zhang et al., 2012a; Bagley et al., 2014; Hu and Dominguez, 2015). Thus, identifying and investigating the variation of precipitation processes due to LUCC is crucial for understanding the regional hydrological cycle, land-atmosphere feedback, and extreme weather events such as droughts (Liu et al., 2015). This, in turn, is essential for understanding exchanges of heat, moisture and momentum in the atmospheric boundary layer. The interactions between the land surface and overlying atmosphere boundary layer take place within a fully coupled land-atmosphere system, where the states (temperature/moisture content) of the air and land surface can strongly influence one another (Huang and Margulis, 2010; Qin and Xie, 2017; Xia et al., 2019).

The surface water and energy exchange processes of ecological transition zones are especially sensitive to LUCC (Cao et al., 2015), thus, these regions are ideal locations to study the effects of LUCC on regional climate. The agro-pastoral ecotone in arid and semi-arid Northwest China faces many ecological problems including sparse vegetation, frequent sandstorms, overgrazing, soil erosion, and ecosystem degradations (Chen et al., 2008; Wu et al., 2013a). Since 1998, Chinese government has initiated several large scale reforestation programs such as "Grain for Green", and "Northern China's Vegetation Belt" programs to return cropland to grassland and forestland, the APENWC has been experiencing a large scale change in land cover (Huang et al., 2007; Wu et al., 2013b; Wei et al., 2018). As a result, surface vegetation change has had strong effects on surface water and energy exchange processes. Liu et al. (2011) indicated a decrease in precipitation in most parts of the farming-pastoral ecotone of Northern China over the last 50 years. Zhao et al. (2017) found that the seasonal mean ET of cropland is greater than that of grassland from 2009 to 2013 in the agro-pastoral ecotone of northern China. Furthermore, there are also strong spatial-temporal variations in surface water and energy factors, due to complex land-atmospheric feedback effects on local climate and hydrological process associated with intense landscape heterogeneity (Huang and Margulis, 2010, 2011; Bryan et al., 2015). Over the last 50 years, meteorological records have shown a rise in temperature and decrease in precipitation in most parts of the agro-pastoral ecotone of northern China, the agrarian sector went through a series of reforms, and changes in government policies on land use have led to extensive changes in land cover (Liu et al., 2011; Li et al., 2015; Zhou et al., 2013). Many studies examined how different land use/cover patterns affected summer temperature in the agro-pastoral ecotone of northern China (Cao et al., 2015; Wei et al., 2018), and the response of crop water consumption to a warming trend and a reduction of precipitation from 1960 to 2007 (Zhao et al., 2013). Feng et al. (2012) studied the spatial and temporal effects of a large ecological restoration project on water yield across the Loess Plateau region in northern China. In this dynamic, heterogeneous agro-pastoral ecosystem, cropland, grassland, shrub lands and artificial forests constantly change back and forth, the surface water-energy exchanges are more complex and dynamic, but poorly understood, little is done on how LUCC affects energy balance and water cycle and land surface-atmosphere interactions at the regional scale in the APENWC.

In addition, in the arid and semi-arid region of China, ground meteorological observatory sites are sparsely distributed, it is a challenge to obtain high-resolution spatial and temporal weather and land surface observation data. Some high-resolution data can be obtained from satellite-based sensors such as the MODerate resolution Imaging Spectroradiometer (MODIS) and Soil Moisture Active Passive (SMAP) sensors. However, such data only provide 'snapshots' of conditions during the transit of the satellites. Regional climate models are potentially effective tools for understanding spatial-temporal distributions of the key local land surface-atmosphere interactions (Gao et al., 2017; Silverman et al., 2013; Wagner et al., 2016; Xia et al., 2017). However, previous studies show that simplified general circulation models cannot fully simulate fine-scale land surface and atmospheric states and often do not accurately capture the detailed diurnal land-atmosphere interactions, thus, Huang and Margulis (2010) advocated use of a fully coupled land surface model and atmosphere boundary layer model for exploring land-atmosphere interactions more accurately. In recent years, a state-of-the-art regional weather research and forecasting model (WRF) has been increasingly used to dynamically downscale General Circulation Model results to spatial resolutions of around 10–40 km and simulate land surface-atmosphere interactions. Numerical research has indicated that the model can effectively simulate land surface water and energy exchange processes (Wan and Xu, 2011; Wen et al., 2012; Yuan et al., 2017).

In this study, we fill a gap in our understanding of response of regional water and energy cycles to LUCC in agro-pastoral ecotone, Northwest China. The objectives of this study are (1) to evaluate the performance of a WRF model in the study region, (2) to determine changes of key surface water-energy factors (LST, ET, and precipitation) caused by the LUCC, and (3) to assess the role of LST, ET, and precipitation in land-atmosphere interactions in the agro-pastoral ecotone, Northwest China.

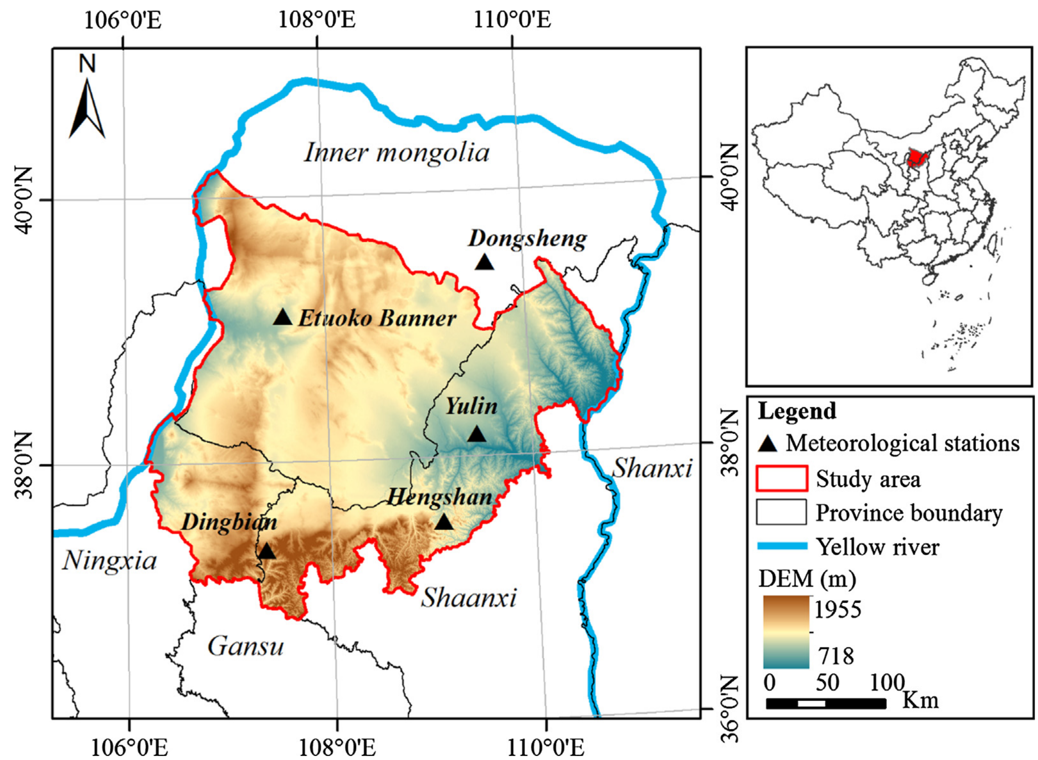

Fig. 1. Location of the agro-pastoral ecotone, Northwest China.

2. Methodology and materials

2.1. Study area

The APENWC extends from ca. 106.228°E to 110.903°E and 36.816°N to 40.194°N (Fig. 1). It is a semiarid region, with an annual average relative humidity of 13%, and mean annual precipitation of 250–450 mm. Main land cover types include grassland, farmland, forest and shrub land, and desert, and dynamic conversion between grassland and farmland occurs frequently (Wei et al., 2018). It is one of the world's largest ecotones, highly sensitive to changes in climate conditions and surface physical properties (Cao et al., 2015). There have been serious historical and recent environmental changes in the APENWC, including grassland degradation, desertification, and biodiversity loss (Li et al., 2018; Wang et al., 2015a). Since 1998, the Chinese government has implemented numerous policies and programs to restore ecosystems and improve environmental protection, such as the large scale 'Grain for Green' program, the Three-North Shelter Forest Program, and Beijing–Tianjin Sand Source Control Program, returning cropland to grassland and forest land (Huang et al., 2007, Wu et al., 2013b).

Since 2000, significant LUCC has taken place in the APENWC, Fu et al. (2011) indicated that the area of woodland and grassland had increased 4.3% and 6.6%, respectively, during 2000–2008. Farmland had decreased about 10.8% during the same period. Meanwhile, area of desert and residential area increased 0.3% and 8.5%, respectively. However, little has been done to assess the impacts of the LUCC on energy and water exchange processes and water cycles in the region. Thus, this study aims to better understand effects of these large scale ecosystem rehabilitation programs and LUCC on regional water-energy exchange processes.

2.2. Model description

The WRF model was developed collaboratively by the US National Center for Atmospheric Research (NCAR) and National Centers for Environmental Prediction (NCEP). The WRF is a next-generation mesoscale numerical weather prediction system designed for both atmospheric research and operational forecasting applications. It features two dynamic cores, a data assimilation system, and a software architecture supporting parallel computation and system extensibility (Skamarock et al., 2008). It offers multiple options for parameterizing subgrid-scale physical processes (e.g., convection, microphysics, radiation) and the planetary boundary layer schemes. In addition, land surface models (LSMs) compute heat and moisture fluxes over the surface, providing lower boundaries for atmospheric models. A detailed description of the model can be obtained at http://www.mmm.ucar.edu/wrf/users/. The non-hydrostatic WRF version 3.8.1 modeling system was used in this study.

2.3. Model configuration and experimental design

The simulation domain is shown in Fig. 1. A single-nested grid system is used in this study, the domain is centered at 38.5° N and 108° E with dimensions of 60 × 60 horizontal grid points with spacing of 10 km. The 6-h, 0.5° × 0.5°NCEP Climate Forecast System Reanalysis (CFSR) (https://rda.ucar.edu/datasets/ds093.0/) from the NCEP provided initial and lateral boundary conditions for the WRF model.

In order to evaluate the performance of WRF model and obtain a suite of optimal physical schemes for the WRF to best simulate land surface processes in the arid region of Northwestern China, we conducted a series of WRF testing runs using its sixteen microphysics, four cumulus and six planetary boundary-layer schemes. To identify the optimal suite schemes for our domain, sensitivity tests were first conducted covering June-October 2010, using standardized deviations (SDs), correlation coefficient, and root mean square errors (RMSEs) to compare precipitation and temperature patterns.

After obtaining the optimal physical schemes of simulation through test experiments, we re-ran the WRF model by changing the land use data of the model (Fig. 2). The simulation time began at 1200 UTC September 1, 2009, and ended at 1200 UTC December 31, 2010, the first three months from September 1, 2009 to November 30, 2009 were

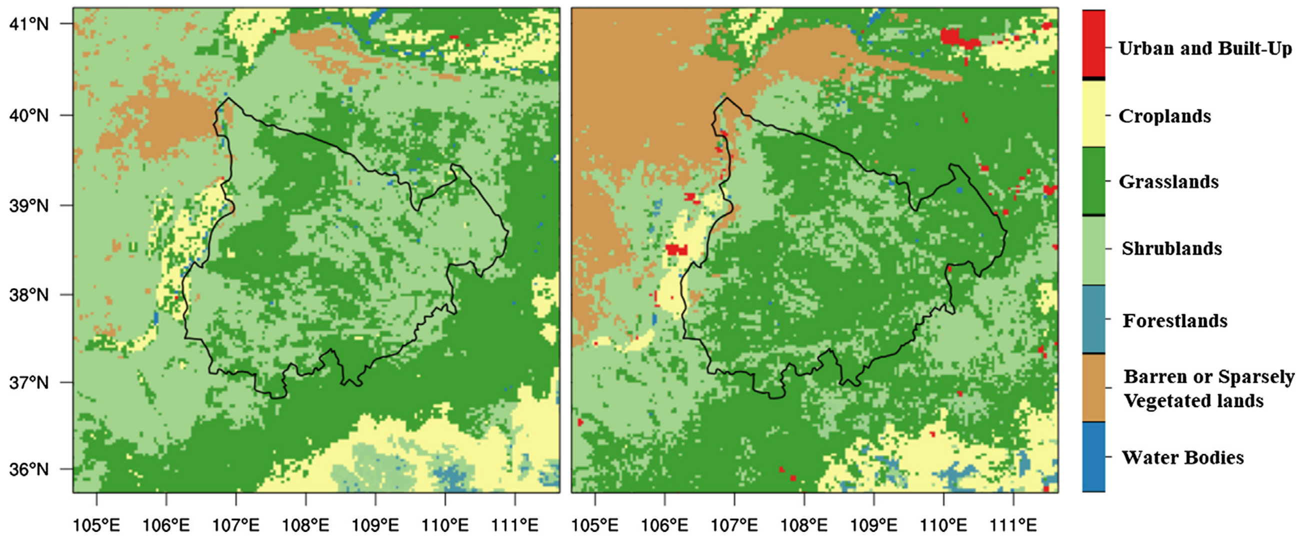

Fig. 2. Dominant land use categories in 1993 (left) and 2010 (right).

considered as spin-up time and therefore excluded from the analysis. We carried out two simulation experiments to look into the response of surface water and energy to LUCC. Two land use/cover datasets were used in the experiment from September 1, 2009 to December 31, 2010 (Exp1993: 1993 land use/cover data and Exp2010: 2010 land use/cover data were used in the experiments), two simulations used the same schemes and climate-driven data.

2.4. Validation datasets

In order to verify and evaluate the simulation results, we selected five national weather stations' (Dongsheng, Henshan, Yulin, Dingbian, and Etuoke Banner stations) data set provided by China Meteorological Administration (http://data.cma.cn) in our study area to verify simulated 2 m air temperature and precipitation, and MODIS land products were selected to validate land surface temperature (https://lpdaac.usgs.gov/dataset discovery/modis). The MODIS land surface temperature product is an 8-daily composite, including daytime and nighttime, configured onto a 0.05 (~5.6 km) latitude/longitude grid. Furthermore, China Meteorological Forcing Dataset (http://westdc.westgis.ac.cn/) was chosen for collaborative evaluation.

2.5. Model evaluation criteria

To assess the model's performance in terms of the fit between observed and simulated data, we used three criteria advocated by Taylor (2001), Moriasi et al. (2007) and Gleckler et al. (2008): the correlation coefficient (R), standard deviation (SD), and normalized standard deviation (NSD):

$$R = \frac{\sum_{i=1}^{n}(X_i^{obs} - \bar{X}_i^{obs})(X_i^{sim} - \bar{X}_i^{sim})}{\sqrt{\sum_{i=1}^{n}(X_i^{obs} - \bar{X}_i^{obs})^2}\sqrt{\sum_{i=1}^{n}(X_i^{sim} - \bar{X}_i^{sim})^2}} \tag{1}$$

$$SD = \sqrt{\frac{1}{n}\sum_{i=1}^{n}(X_i - \bar{X})^2} \tag{2}$$

$$NSD = \frac{SD_{sim}}{SD_{obs}} \tag{3}$$

Here, X_i^{obs} and X_i^{sim} are the observed and simulated values for month (or year) i, while $\bar{X}_i^{obs}$ and $\bar{X}_i^{sim}$ are the average observed and simulated data during the simulation period, SD_{obs} and SD_{sim} are the observed and simulated values of standard deviation (SD).

2.6. The vertical integrated water vapor flux

To evaluate the impacts of moisture transportation on precipitation in the APENWC, the precipitable water and vertically integrated horizontal water vapor fluxes were calculated by the following equation:

$$w = -\frac{1}{g}\int_{P_{surface}}^{200hPa} q\ dp \tag{4}$$

$$Q = -\frac{1}{g}\int_{P_{surface}}^{200hPa} Vq\ dp \tag{5}$$

where w and Q are the precipitable water and vertically integrated water vapor flux, q, g, $P_{surface}$, and V represent the specific humidity, gravity, surface pressure, and horizontal wind vector, respectively (Zhang et al., 2017).

2.7. Model evaluation

In this study, we focus on three categories of the physical parameterization schemes: the microphysics, planetary boundary layer and cumulus schemes, all of which are directly related to regional water and energy exchanges (Rajeevan et al., 2010; Ács et al., 2014; Teixeira et al., 2014).

Fig. 3 shows Taylor diagrams for rainfall and 2 m air temperatures. The arcs in the diagrams show correlation coefficients, while the horizontal and vertical axes indicate the ratio of the standard deviation (SD) of the simulated data to the observations. All simulations show high correlation coefficients (0.8–0.95) for 2 m air temperatures, but the simulated precipitation is sensitive to all physics schemes, with normalized standardized deviations of 0.5–0.8 and correlation coefficients of 0.3–0.8.

We selected a set of physical options for the WRF model, based on comparisons of the simulation outputs with the recorded 2 m air temperature and rainfall data (Fig. 4). The planetary boundary layer processes were resolved with the UW (University of Washington) boundary layer scheme from CAM5 (CESM 1_0_1). The microphysics was described with the Thompson scheme (new for V3.1), and the cumulus clouds was simulated with A newer Tiedtke scheme. The Rapid Radiative Transfer Model (RRTM) and Dudhia shortwave radiation scheme were used to calculate long wave and short wave radiation and their transfer within the atmosphere, respectively. The Community Land Model version 4 (CLM4, adapted from CAM) with 10 soil layers was used to simulate land surface processes within the WRF.

After selecting the above options, we re-ran WRF model with

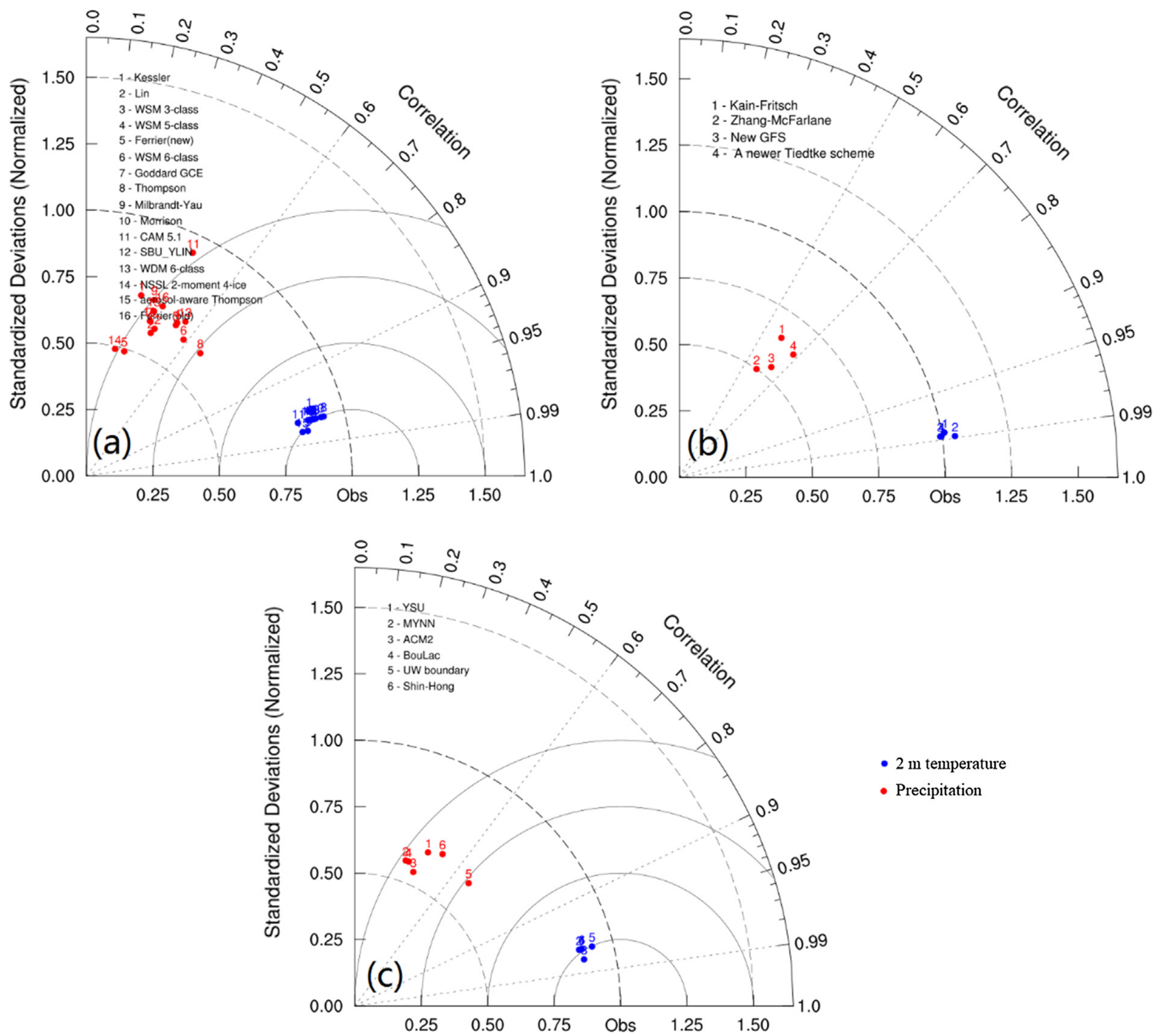

Fig. 3. The summaries of different schemes of Taylor diagrams for 2 m temperature (blue dot) and precipitation (red dot) ((a) for microphysics option; (b) for cumulus option; (c) for boundary-layer option). (For interpretation of the references to colour in this figure legend, the reader is referred to the web version of this article.)

simulation time beginning at 12:00 September 1, 2009, and ending at 12:00 December 31, 2010. Fig. 4 shows the temporal variation and scatter diagram for precipitation and land surface temperature, 2 m air temperature. The coefficients of determination (R^2 values) for monthly accumulated precipitation and air/surface temperature are 0.71 and > 0.9, according to the scatter diagram. The simulation results show a higher consistency with the observed values in the temporal pattern of temperature and precipitation. The results indicate that the WRF model can accurately simulate regional water and energy processes in the APENWC.

3. Results

3.1. LUCC from 1993 to 2010

The generated LUCC matrix and associated changes in land cover assigned to specific land use categories in the study period in the APENWC are shown in Table 1. Fig. 2 shows the distribution of the land cover in 1993 (left) and 2010 (right), and Table 2 shows changes in areas of land-use categories from 1993 to 2010. Based on the changes of land use/cover listed in Table 1 in the APENWC, the most obviously increased land cover types were the grasslands and barren land, increasing by 8.22% and 13.22%, respectively, as a result of conversion from croplands with 5.86% and shrublands with 12.49% into grasslands, and from shrublands with 13.01% into barren or sparsely vegetated land; the total croplands decreased by 5.06%, and shrublands decreased by 17.25% (Tables 1 and 2).

3.2. Land surface temperature response

As discussed above, the energy and water exchanges between the land surface and atmosphere (e.g., sensible and latent heat fluxes) are largely controlled by the difference between the land surface temperature and near-surface air temperature (Hagos et al., 2014; Cao et al., 2015; Boone et al., 2016). Due to the lack of regional scale surface temperature records for Northwest China, previous studies on effects of land use change on surface temperature in the region have generally relied on remote sensing data. However, such data only provide 'snapshots' of conditions during the transit of satellites, and thus provide limited indication of temporal patterns of surface temperature. Therefore, we ran the WRF model with two land use data sets of 1993 and 2010 as inputs to eliminate the influence of external conditions and isolated changes in surface temperature directly caused by the LUCC.

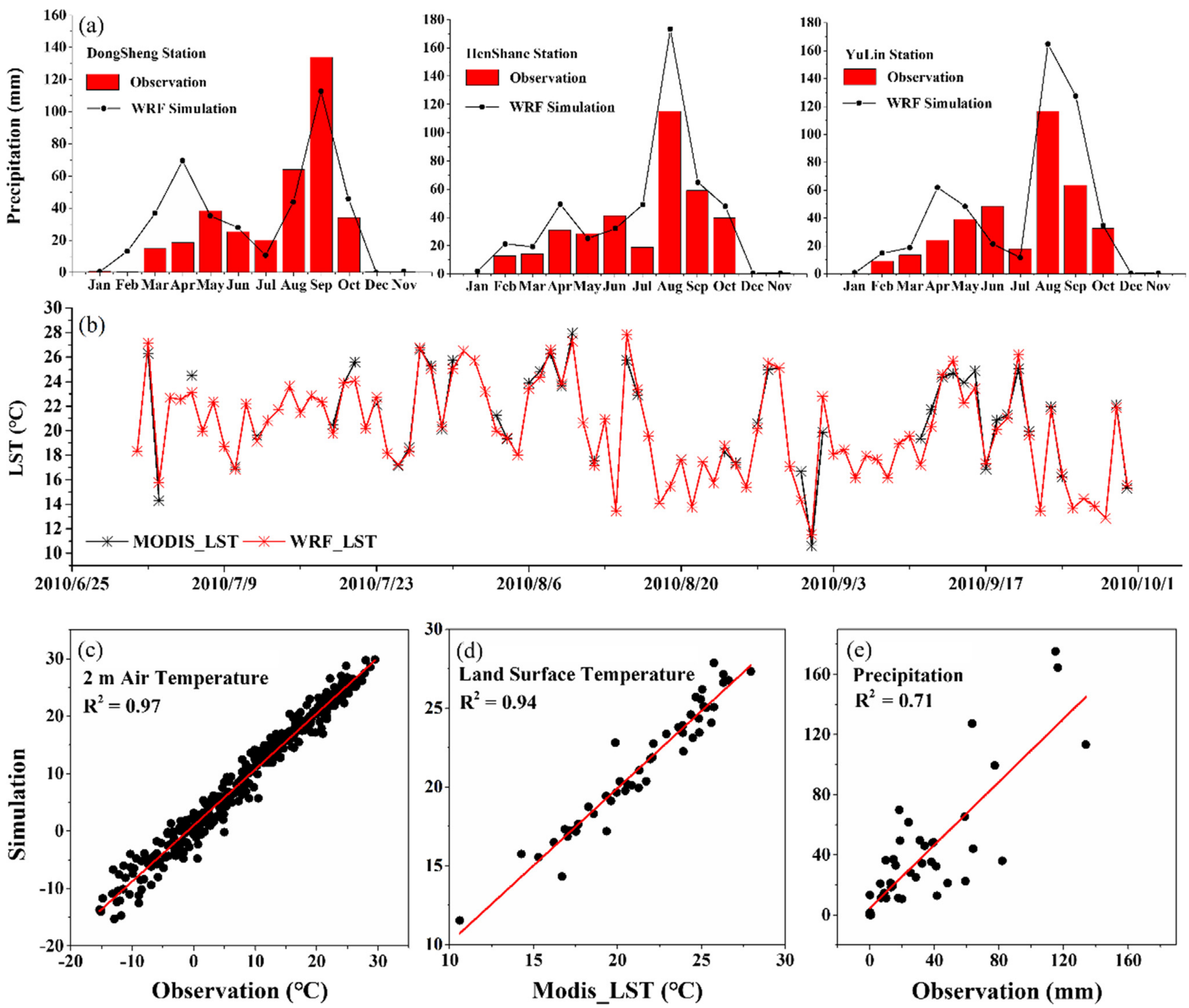

Fig. 4. Temporal variation of simulated and observed precipitation ((a), in mm) and land surface temperature ((b), in °C) and scatter diagrams for 2 m air temperature ((c), in °C), land surface temperature ((d), in °C), and precipitation ((e), in mm).

Spatially averaged seasonal differences in simulated LST between Exp1993 and Exp2010 (d Ts = LST2010 – LST1993) (Fig. 5) were −0.45, −0.99, −0.24 and −0.33 °C in spring (MAM: March, April & May; MAM), summer (JJA: June, July & August; JJA), fall (SON: September, October & November; SON), and winter (DJF: December, January & February; DJF), respectively. The minimum and maximum differences were −3.57 and 1.40 °C, respectively, in summer. As can be seen in Fig. 5, due to the transformation of a large area of shrublands into grassland, the average monthly LST in this area decreased, especially in spring and summer, and in both seasons, the LST was clearly higher in barren land than in grassland. The spatial distribution of LST indicates that the strongest reductions in temperature were in areas

Table 1
The LUCC matrix in 1993–2010 (%).

LULC1993	LULC2010 Urban and Built-up Land	Croplands	Grasslands	Shrublands	Forestlands	Barren or Sparsely Vegetated Land	Water Bodies	1993
Urban and Built-up Land	0.04	~	~	~	~	~	~	0.04
Croplands	0.34	6.27	5.86	0.95	0.19	0.01	0.03	13.65
Grasslands	0.37	0.86	26.98	8.11	0.92	0.16	0.07	37.47
Shrublands	0.13	1.06	12.49	14.92	0.18	13.01	0.05	41.84
Forestlands	0.03	0.32	0.16	0.14	0.78	~	~	1.43
Barren or Sparsely Vegetated Land	~	~	0.02	0.33	~	4.56	~	4.91
Water Bodies	0.01	0.08	0.21	0.14	~	0.03	0.19	0.66
2010	0.92	8.59	45.72	24.59	2.07	17.77	0.34	100

Note: (1) the data in Table 1 is the percentage of regional area transfer to the total area of regional land; (2) the last column and the last row represent the percentage of each category in 1993 and 2010, respectively.

Table 2
The variation of land-use in 1993–2010 (%).

Land use category	Period reduction	Period increase	Net increase
Urban and Built-up Land	0	0.88	0.88
Croplands	7.38	2.32	−5.06
Grasslands	10.49	18.74	8.25
Shrublands	26.92	9.67	−17.25
Forestlands	0.65	1.29	0.64
Barren or Sparsely Vegetated Land	0.35	13.21	12.86
Water Bodies	0.47	0.15	−0.32

where shrublands were transformed into grasslands, but this trend was weak or non-existent in winter. Conversely, the strongest increases were in areas where grasslands were transformed into shrublands or barren land, in summer. The LST time series indicate that the daily surface temperature was maximal and minimal at approximately 1400 and 0500, respectively.

To improve our understanding of effects of changes in albedo on LST, we plotted the relationship between changes in LST (d Ts: Ts2010 – Ts1993) and albedo (d albedo: albedo2010 – albedo1993) for all grid points within the regions (Fig. 6). The results show a significant negative correlation, with R^2 values of 0.91, 0.94, 0.85 and 0.43 in spring, summer, fall and winter, respectively. As shown in Fig. 7, the simulations indicate a clear tendency for the annual mean surface temperature to decline during the study period due to increases in albedo.

3.3. Evapotranspiration response

ET, an important element of both the hydrological cycle and surface energy balance, is affected by changes in both LUCC and climate. Here, we only consider the effects of the LUCC, by keeping the atmospheric forcing field constant, thereby isolating effects of the LUCC on ET. The spatial distribution of seasonal difference in ET between the two simulations (d ET: ET2010 – ET1993) is shown in Fig. 8. The spatially weighted averaged differences of all grids are −1.15, 19.79, −13.22 and −0.96 mm for spring, summer, fall and winter, respectively. Conversion of shrublands to grasslands resulted in an increase in ET in summer, and a decrease in fall. Conversely, conversion of grassland to shrublands resulted in a decrease in ET in summer.

As shown in Fig. 9, we also found that differences in evapotranspiration (d ET: ET2010-ET1993) and albedo (d albedo: albedo2010 – albedo1993) in the two simulations (for all grid points within the region) were negatively correlated in spring, fall and winter

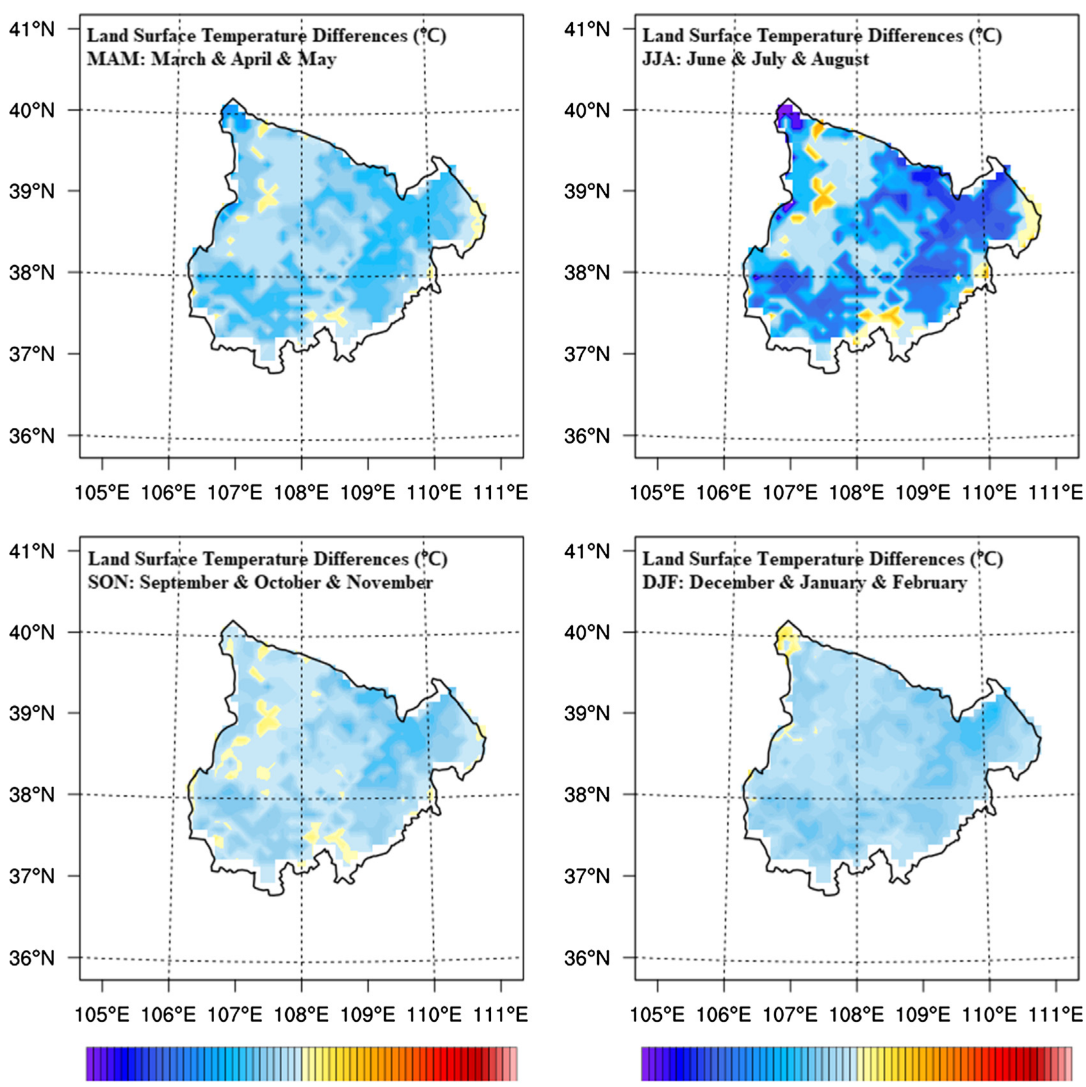

Fig. 5. Differences in mean seasonal land surface temperature (LST, °C) between the simulations with 2010 and 1993 land use data (LST2010 - LST1993) during MAM, JJA, SON and DJF (MAM: March & April & May; JJA: June & July & August; SON: September & October & November; DJF: December & January & February).

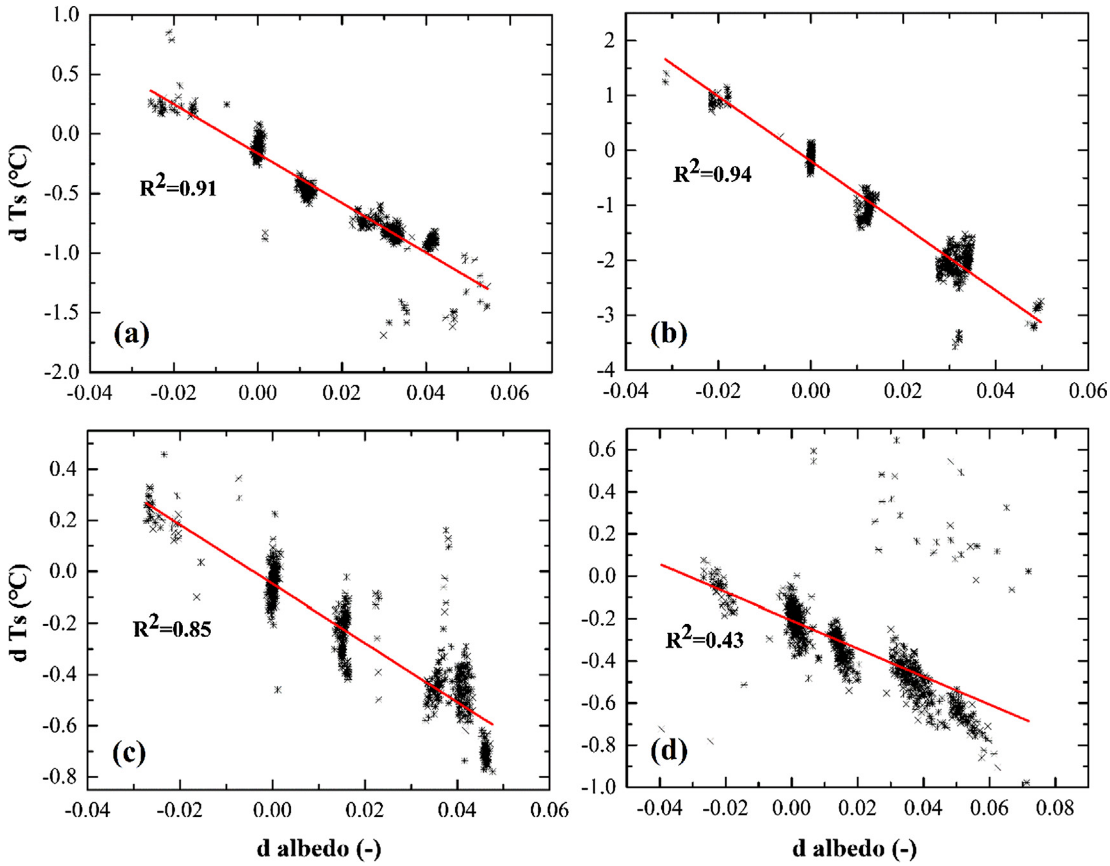

Fig. 6. Relationships between differences in surface temperature (d Ts, °C) and surface albedo (d albedo) in the simulations with 2010 and 1993 land use data for all grid points of the region. Regression lines are shown in red. ((a) for MAM: March & April & May; (b) for JJA: June & July & August; (c) for SON: September & October & November; (d) for DJF: December & January & February). (For interpretation of the references to colour in this figure legend, the reader is referred to the web version of this article.)

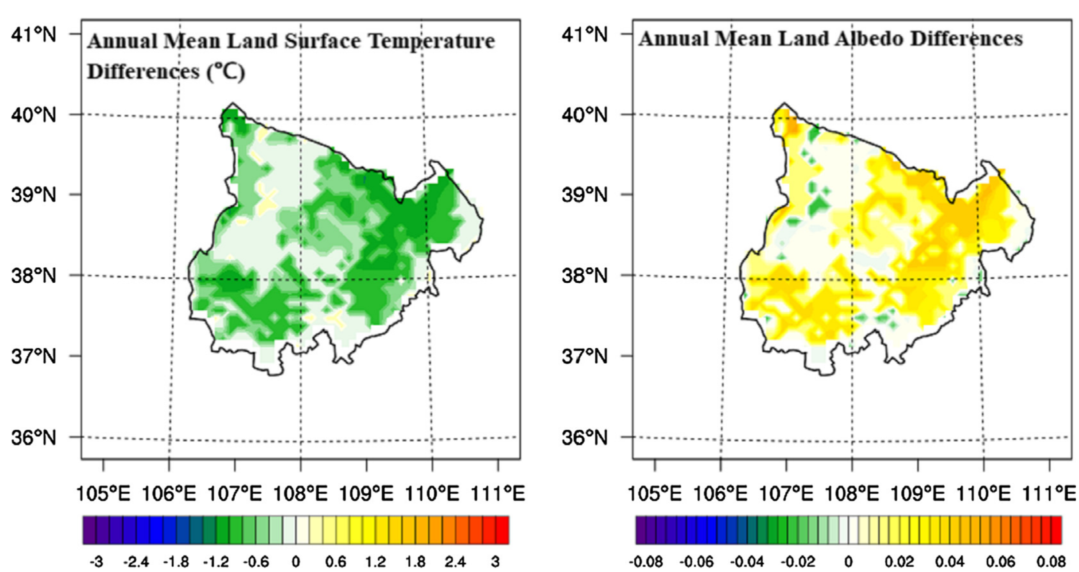

Fig. 7. Differences in annual mean surface temperature (d Ts; °C) and corresponding differences in surface albedo (d albedo) between 1993 and 2010 according to the simulations.

(R^2 values, 0.13, 0.72 and 0.14, respectively). However, they were significantly positively correlated in summer (R^2 = 0.49).

3.4. Precipitation response

The seasonal precipitation and vertically integrated water vapor simulation are shown in Fig. 10. The simulated precipitation was concentrated in the east of the region, and most of the moisture came from the west in spring (MAM). In summer (JJA), precipitation is mainly concentrated in the southeast, the majority of the moisture came from the south, the greater East Asian monsoon and Indian Ocean monsoon become the major moisture source. In fall (SON), the precipitation

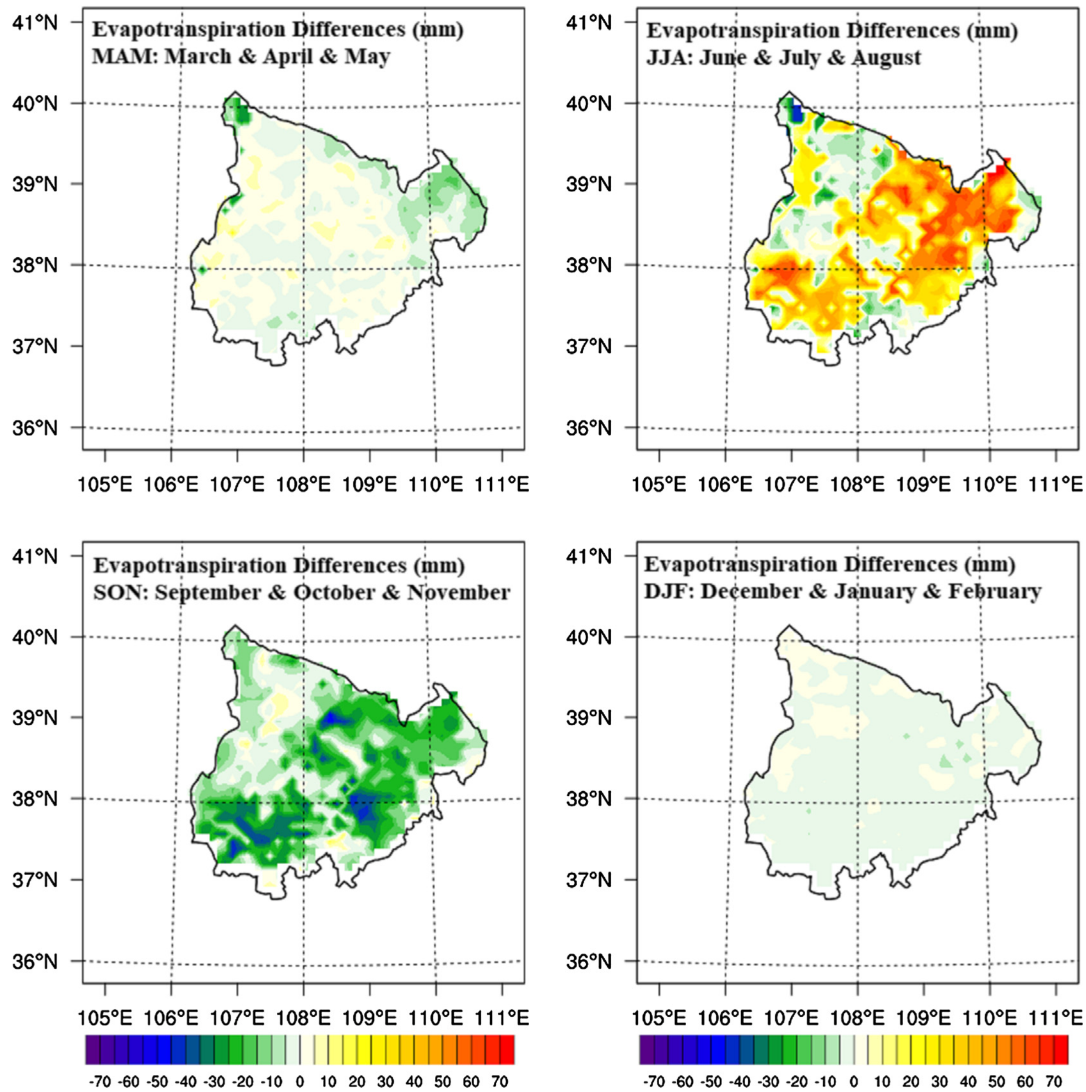

Fig. 8. Differences in ET (mm) between the simulations with 2010 and 1993 land use data (ET2010 - ET1993) during MAM, JJA, SON and DJF (MAM: March & April & May; JJA: June & July & August; SON: September & October & November; DJF: December & January & February).

pattern was similar to the spring pattern, and the majority of the moisture came from the west and southwest. In winter (DJF), the pattern of moisture sources was similar to the spring pattern, but there was very little precipitation.

To better understand precipitation's response to the LUCC, seasonal moisture sources must be characterized. Thus, we investigated the seasonal changes in moisture sources and compared their differences during spring, summer, fall, and winter. Fig. 11 shows differences in the spatial distributions of simulated seasonal precipitation during the four seasons (with vectors representing the differences in seasonal vertically integrated water vapor fluxes). As can be seen from the Fig. 11, precipitation is very sensitive to the LUCC, with spatially averaged differences of −2.30, −7.31 and −7.80 mm in spring, summer, and fall, respectively (but no difference in winter, when there was extremely little precipitation in the region).

The differences in vertically integrated seasonal water vapor flux can help us identify regions that contributed most to the changes in moisture transport. Generally, the more moisture is transported into a region, the more moisture source contributes to the precipitation over the region, and vice versa (Zhang et al., 2017). From Fig. 10, the moisture over the region came mainly from the westerlies, East Asian monsoon and Indian Ocean monsoon. However, from Fig. 11, according to the difference in the moisture between the two simulations (Exp2010-Exp1993) and comparing the Fig. 10, the moisture over the region declined. In spring (MAM), the moisture came from the westerlies decreased in the west of the region, but this change is very weak. In summer (JJA), the moisture from the East Asian monsoon and Indian Ocean monsoon decreased in the south of the region, however, in the north, the moisture increased, and the area within the APENWC contributed greatly to providing the extra moisture transported into the north of the region. In fall (SON), the pattern was similar to the spring pattern, and the moisture from the west decreased in the west of the region, but there is an increase in the east of the region. Negative differences in the moisture flux mean more moisture was transported away from the region, resulting in reduced in moisture in areas within the region.

There are many connections between land surface characteristics and water cycle, from the perspective of atmospheric moisture balance, the reduction in precipitation is a result of changes in local surface ET and atmospheric moisture convergence (Wei et al., 2016). Fig. 12 shows the relationship between precipitation change and the change in ET. The points in Fig. 12 would fall on the lines of 1:1 if all the precipitation change is explained by changes in ET. However, this was not the case, and coefficients of determination between d precipitation and d ET were 0.349, 0.001, 0.260 and 0.063 in spring, summer, fall, and winter, respectively. These findings show that ET was not the only factor that

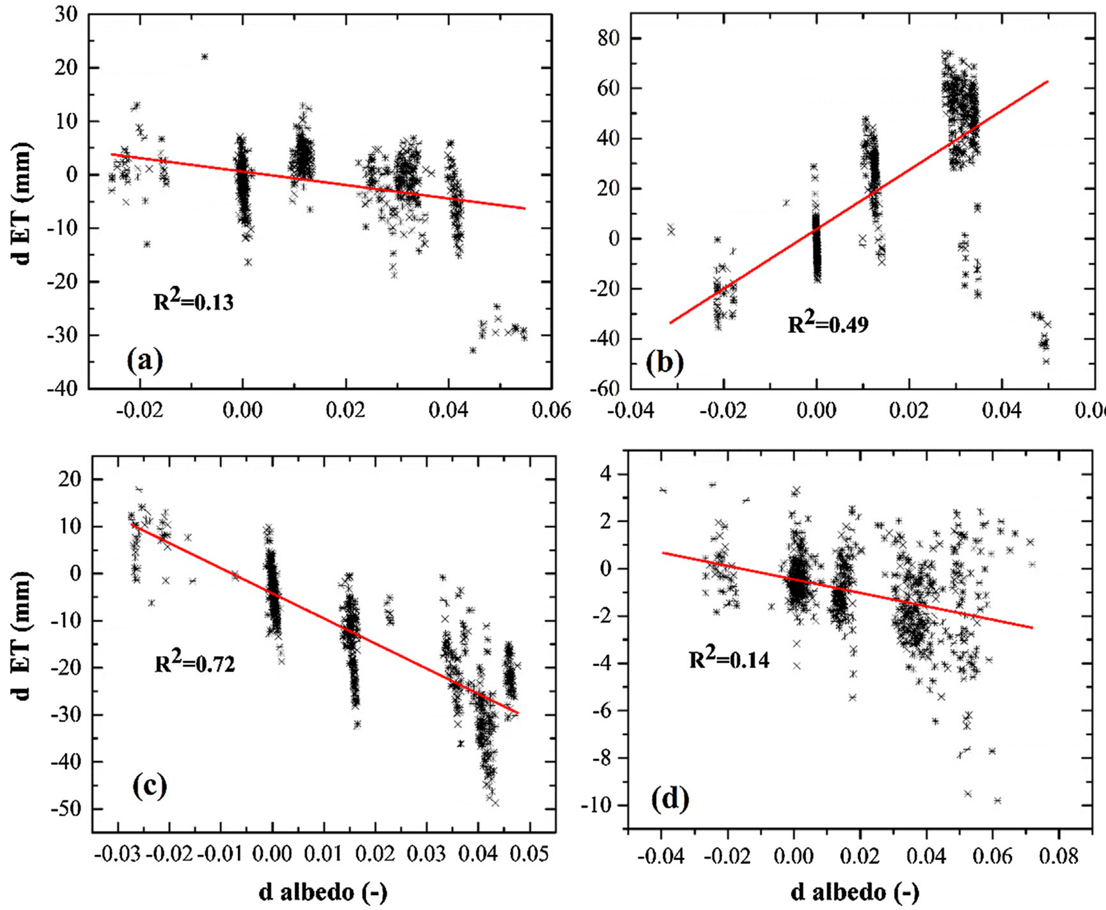

Fig. 9. Relationships between differences in evapotranspiration (d ET, mm) and surface albedo (d albedo) in the simulations with 2010 and 1993 land use data for all grid points of the region. Regression lines are shown in red. ((a) for MAM: March & April & May; (b) for JJA: June & July & August; (c) for SON: September & October & November; (d) for DJF: December & January & February). (For interpretation of the references to colour in this figure legend, the reader is referred to the web version of this article.)

affected precipitation, and the LUCC affects availability of moisture not only through changes in ET, but also (more importantly) through changes in atmosphere circulation and vapor flux transport (Hagos et al., 2014; Hua et al., 2016; Guo et al., 2018).

4. Discussion

In this study, we first determined the optimal suite of WRF physics schemes by sensitivity tests. We then used 6-h, 0.5°×0.5° NCEP Climate Forecast System Reanalysis (CFSR) data, and land use products of 1993 and 2010 to drive WRF simulations of land surface water and energy exchange processes associated with the different land use and land cover types in the APENWC from September 2009 to December 2010. Results of the sensitivity analysis, and comparison of simulations and observations clearly show that the WRF model can accurately simulate regional water and energy processes in the study region. In addition, data presented in Fig. 2, and Tables 1 and 2, show that land use and land cover changed substantially between 1993 and 2010 in the region. The strongest changes were increases in grasslands and barren or sparsely vegetated land, with accompanying reductions in croplands, associated with the large scale national Grain for Green program. Then, we analyzed responses of surface water and energy cycles to the LUCC in the region.

4.1. Energy cycle

The water and energy exchange processes combine the water and energy transfer of surface vegetation, soil and atmospheric boundary layer into a whole, are the focus and hotspot of current earth system science research. In our study, we analyzed the response of surface temperature, evapotranspiration, and precipitation to the land use and land cover change. Our analysis of responses of surface temperature, ET, and precipitation to the LUCC show that the LUCC affected surface temperatures by altering the land surface albedo, which strongly influences energy fluxes between land surfaces and the atmosphere, as increases in albedo reduce the energy available for turbulent fluxes of heat and moisture across the boundary (Boone et al., 2016). Hence, in parts of the region where shrublands were transformed into grasslands, land surface temperature decreased, and vice versa. Surface temperature is an important determinant of sensible and latent heat fluxes, and thus amounts of energy that are vertically transported into the ground (Sohrabinia et al., 2012). Changes in surface temperature also influence local ET.

ET is an important component of both the hydrological cycle and surface energy balance. Previous studies have shown that LUCC affects ET by changing water-energy factors such as air temperature, wind speed, and relative humidity (Dias et al., 2015; Li et al., 2017; Olchev et al., 2008). In general, ET in a region has two main contributors: (1) soil evaporation (and/or water body) and (2) vegetation transpiration/interception within the region. In the APENWC, the shrublands belong to open shrublands, its coverage is less than 20%, but when the shrublands transformed into grassland, the grassland coverage is 60–90%, or even more. In spring and winter, due to low temperature, short sunshine durations and dormant vegetation, soil evaporation is the main contributor of the total ET in the study region, Thus ET is low and the variation is very small. However, when the shrublands

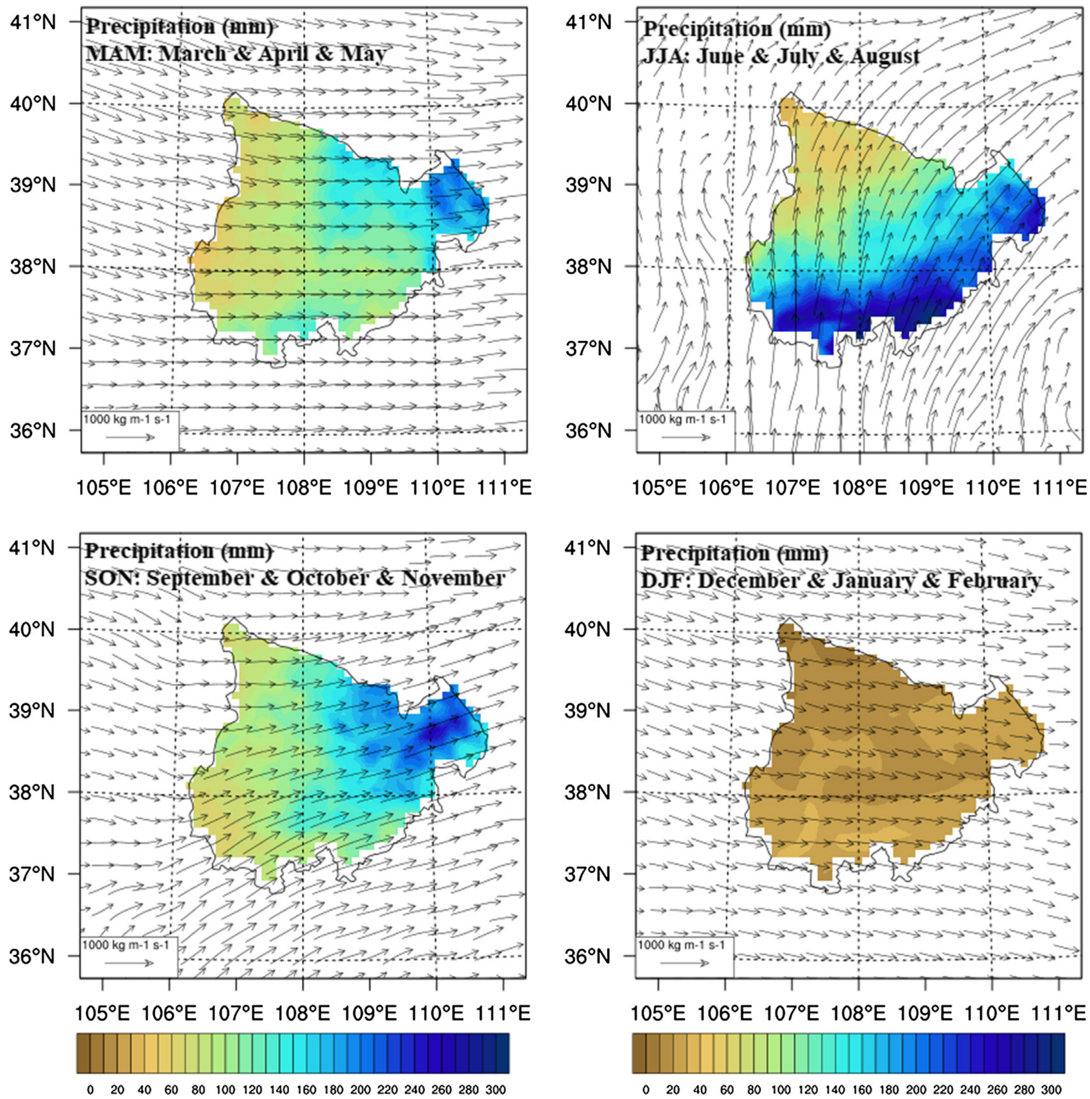

Fig. 10. Simulated precipitation (mm) during MAM, JJA, SON, and DJF. The vectors represent the climatological seasonal vertically integrated water vapor flux during MAM, JJA, SON, and DJF (MAM: March & April & May; JJA: June & July & August; SON: September & October & November; DJF: December & January & February).

transformed into grasslands, in summer, ET is much higher and largely derived from plant transpiration and interception evaporation, which accounts for most of the total ET. Besides, summer is the rainy season in the APENWC, due to shrub's root architecture, higher and deeper infiltration and lateral redistribution of water existed beneath shrublands as compared with grassland, in the shrublands, rainfall partition induced by shrub's root architecture results in preferential water flow into deep soil layer compared with grassland. (Li et al., 2013). However, in arid/semi-arid areas, ET is limited mostly by soil water (Li et al., 2016), summer rainfall causes the shrublands soil to store more water in deeper soil, in the fall, soil evaporation is greater in open shrublands compared with grassland, but, in areas where shrublands were transformed into grasslands, the grasses withered, causing major drops in plant transpiration and inhibition of soil evaporation in the fall, therefore, the total ET sharply decreased compared with shrublands.

4.2. Water budget

Increases in ET and reductions in precipitation will lead to soil drying, and may exacerbate droughts in summer across the region. Feng et al. (2012) found that water yield in 38% of the Loess Plateau area might have decreased (1–48 mm per year) as a result of LUCC. Zhang et al. (2012b) indicated that the region located in the upper reaches of the Yellow River experienced upward trends in the total drought area. In addition, Liu et al. (2016b) found that the southwest of the Loess Plateau has a significant increasing trend of drought severity based on the Standardized Precipitation Evapotranspiration Index. The increase in drought area may cause damage to agricultural production and regional food security. Our finding is similar to those found in the Loess Plateau and the upper reaches of the Yellow River Basin in Northwest China.

Knowledge of the spatial-temporal distribution of water is crucial for the sustainable development of agriculture and other socio-economic activities (Hagos et al., 2014). Precipitation is the main source of moisture in the APENWC, and our results show that the potential feedback of the LUCC on local climate may have reduced precipitation. To study LUUC's effects on precipitation in detail, we first considered ET and water vapor transportation. Fig. 13a shows various fluxes associated with precipitation processes in the APENWC. In general, precipitation (P) has two sources in a region: (1) water vapor evaporated within the region contributed to precipitation, called recycled precipitation (P_r) and (2) water vapor transported into the region from outside contributed precipitation, called advective precipitation (P_a), so the P is the sum of P_a and P_r. The upward evaporative flux is

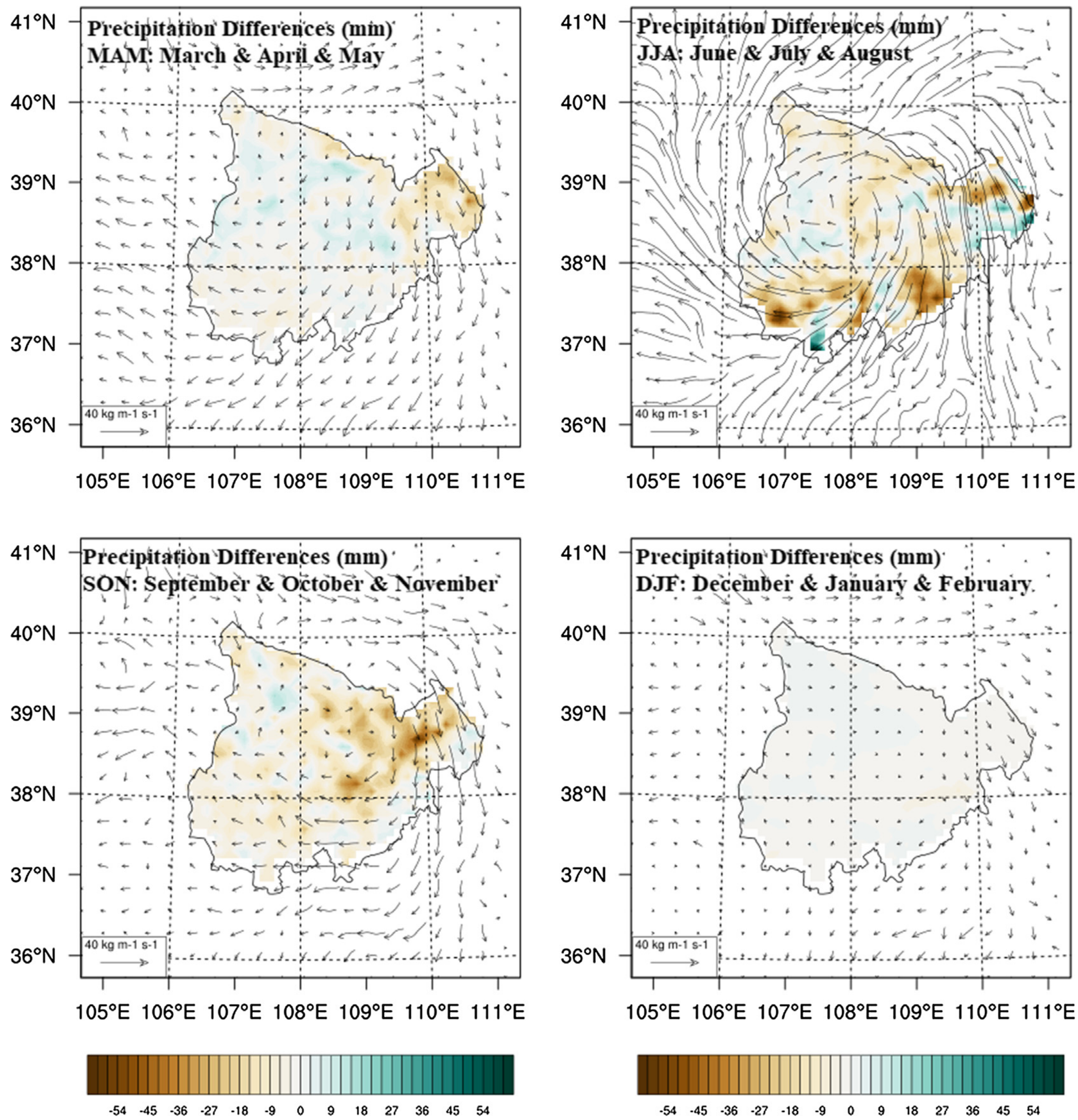

Fig. 11. Differences in precipitation (mm) in the simulations with 2010 and 1993 land use data (P2010 - P1993) during MAM, JJA, SON and DJF. The vectors represent the difference of the seasonal vertically integrated water vapor flux between the two experiments during MAM, JJA, SON and DJF (MAM: March & April & May; JJA: June & July & August; SON: September & October & November; DJF: December & January & February).

represented by E, and inflow and outflow of advective moisture is represented by F_{in} and F_{out}, respectively. In our two experiments, we changed land use data of the WRF model, and control F_{in} to remain unchanged. Subsequent analysis revealed a positive correlation between changes in precipitation and ET, with R^2 values of 0.394, 0.001, 0.260, and 0.063 in spring, summer, fall, and winter, respectively, indicating that ET makes a contribution to precipitation in the region, and the LUCC changes recycled precipitation (P_r). The ratio of precipitation contributed from water vapor evaporated within the region (P_r) versus the total precipitation (P) is known as the precipitation recycling ratio (PRR), this ratio indicates the importance of the interactions between the atmosphere and land surface, and is an indicator of general climatic sensitivity to LUCC (Brubaker et al., 1993; Dominguez et al., 2006; Eltahir and Bras, 2010). Fig. 13b shows the temporal variability of PRR in the APENWC, the PRR is 0.15–0.46 and averaged PRR is 0.273 and 0.268 in different land use data experiment of 1993 and 2010, implying that about 27% (averaged two PRR) of the precipitation comes from the local ET, the other 73% from the external water vapor inflow. In order to further understand how LUCC affects precipitation processes, we considered the primary mechanism of moisture transport. The greater East Asian monsoon, Indian Ocean monsoon, the local and nearby sources in the westerlies were the main moisture contributors to the precipitation in our study region (Fig. 10), based on our simulations. However, due to “Grain for Green”, and “Northern China’s Vegetation Belt” programs, the APENWC has been experiencing a large scale change in land use/cover, in summer, moisture from these sources decreased in the south of the region (Fig. 11c), but in the north the moisture increased, and areas within the APENWC strongly contributed to the additional moisture transported into the north. In summary, surface ET and atmospheric moisture from external water vapor inflows play important roles in precipitation processes and the atmospheric moisture balance in the region, and the LUCC strongly affected both processes.

The results show that the impacts of LUCC on regional water-energy cycle are significant. But the impacts of LUCC on regional land surface water-energy cycle and its variations are still under investigation and not fully understood. Researches have also indicated possible teleconnections between regional LUCC and climate over remote areas (Hasler et al., 2009; Snyder, 2010; Mahmood et al., 2014). For example, the deforestation leads to a regional warming in low-latitude, but a cooling effect in high-latitude (Claussen et al., 2001; Snyder et al., 2004, 2010). Cui et al. (2006) indicated that the impacts of LUCC on the

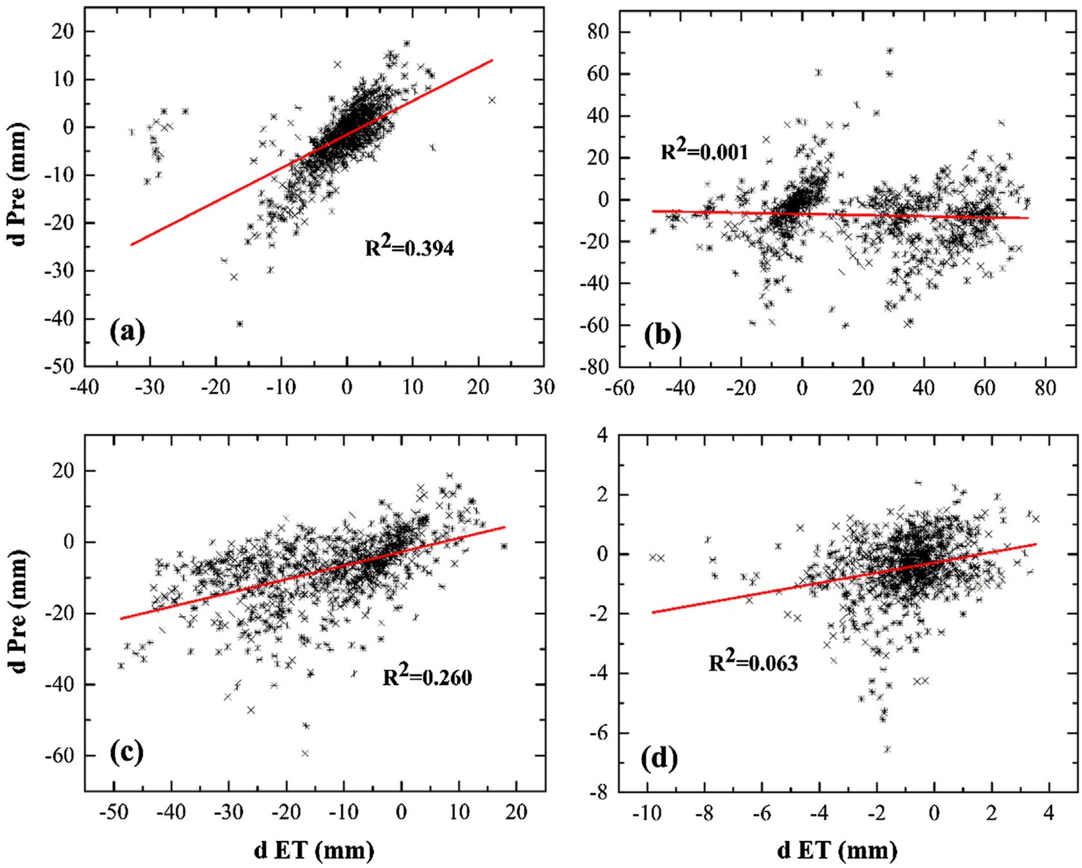

Fig. 12. Relationships between differences in precipitation (d P, mm) and evapotranspiration (d ET, mm) in the simulations with 2010 and 1993 land use data for all grid points of the region. Regression lines are shown in red. ((a) for MAM: March & April & May; (b) for JJA: June & July & August; (c) for SON: September & October & November; (d) for DJF: December & January & February). (For interpretation of the references to colour in this figure legend, the reader is referred to the web version of this article.)

East Asian atmospheric circulation and monsoon precipitation in Tibet Plateau. Sen et al. (2004) also reported that deforestation has an effect of weakening of the monsoon flow over the Tibetan Plateau and eastern China. Thus, the teleconnections should be further investigated to understand their impacts on water and energy cycles.

4.3. Limitations and future research

In the study, we evaluated the performance of WRF simulation using observed temperature and precipitation data, it is important to note limitations associated with uncertainties in the model, which inevitably affect the accuracy of regional outputs. For example, because landscape heterogeneity, what spatial resolution is best in simulating the land surface processes over regional scale remains a challenge in the study region. In addition, surface water-energy exchange processes are complex and cannot be directly monitored, although our results show that the LUCC substantially affected water and energy exchange in the APENWC. Thus, precise description of land surface properties is important for rigorous and accurate numerical modeling simulations. Future studies need to consider these issues in simulating effects of the LUCC on land surface processes in the study region.

5. Conclusions

In this work, we have used a state-of-the-art regional climate model (WRF model) to simulate regional water and energy processes associated with land use and cover in the arid APENWC between 1993 and 2010. We first evaluated the model's performance for the region, and then assessed responses of regional water-energy processes to the LUCC. Our main finding are as follows:

1. The WRF model can accurately simulate regional water and energy processes in the agro-pastoral ecotone.
2. Land use/cover changed substantially between 1993 and 2010 in the study area, the strongest changes were increases in grasslands and barren or sparsely vegetated land associated with the Chinese government's large scale Grain for Green program.
3. Expansion of grasslands reduces energy available for turbulent fluxes of heat, mean surface temperature, and hence soil evaporation. Spatially averaged ET decreased in spring, fall, and winter, but increased in summer. This is because ET derived from transpiration in summer accounts for most total ET, but in other seasons grass is withered, plant transpiration rates are very low, and withered vegetation inhibits soil evaporation.
4. The greater East Asian monsoon, Indian Ocean monsoon, together with local and nearby sources in the westerlies were found to be the most important contributors of moisture to the precipitation. Response of precipitation to the LUCC is extremely sensitive, which has reduced precipitation in the region. The differences in the simulated moisture fluxes also indicate that moisture over this region declined, which means the study region contributed additional moisture from the local ET into the north of the region.

The results suggest that land cover change, especially expansion of grasslands, have reduced land surface temperature in the APENWC. Increases in ET and reductions in precipitation will lead to soil drying, and may exacerbate droughts in summer across the region. The findings provides useful information for formulating optimal strategies for

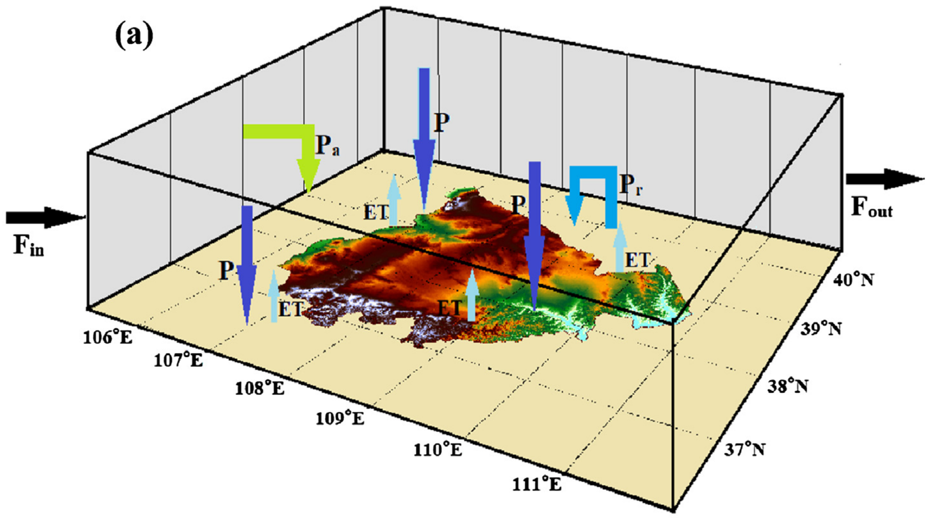

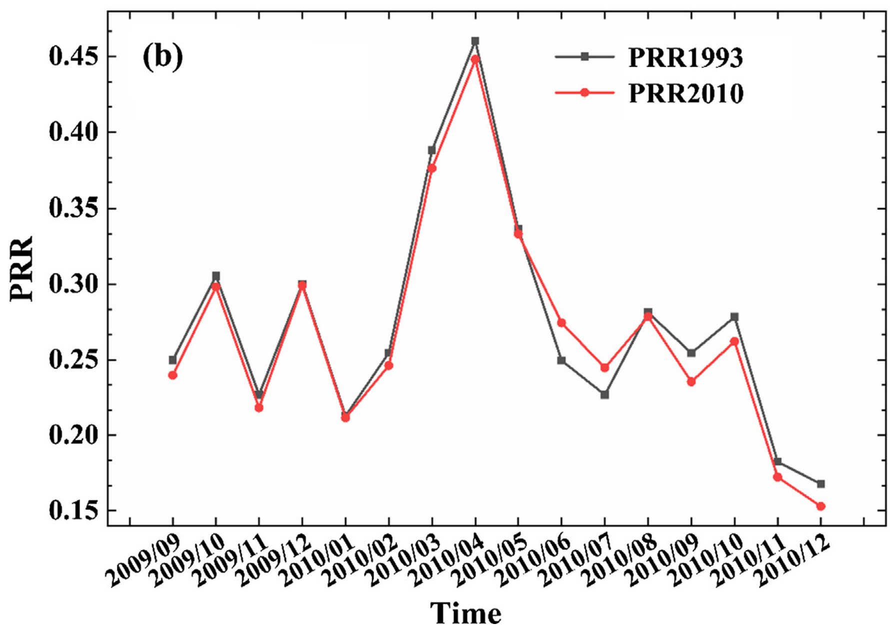

Fig. 13. Schematic representation of regional atmospheric moisture fluxes (a) (P_r, Pa represent the recycled precipitation and advective precipitation, respectively), and (b) temporal variability of the precipitation recycling ratio (PRR) in the APENWC.

animal husbandry, ecological restoration and sustainable development in the APENWC and similar regions.

CRediT authorship contribution statement

Xuejin Wang: Data curation, Formal analysis, Methodology, Software, Validation, Writing - original draft, Writing - review & editing. **Baoqing Zhang:** Conceptualization, Methodology, Writing - original draft, Writing - review & editing. **Xuefeng Xu:** Data curation, Formal analysis. **Jie Tian:** Methodology. **Chansheng He:** Conceptualization, Funding acquisition, Supervision, Writing - review & editing.

Declaration of Competing Interest

The authors declare that they have no known competing financial interests or personal relationships that could have appeared to influence the work reported in this paper.

Acknowledgments

The project is partially funded by the National Natural Science Foundation of China (Grants: 41530752, 91125010, and 41877150) and Scherer Endowment Fund of Department of Geography, Western Michigan University. All WRF simulations were run using advanced computing resources provided by the Northwest A&F University (http://hpc.nwsuaf.edu.cn/index.htm), we are grateful for their support. We also acknowledge kind support by the National Field Station for Grassland Ecosystem in Ordos, Inner Mongolia, China.

References

Ács, F., et al., 2014. Sensitivity of WRF-simulated planetary boundary layer height to land cover and soil changes. Meteorol. Z. 23 (3), 279–293. https://doi.org/10.1127/0941-2948/2014/0544.

Bagley, J.E., Desai, A.R., Harding, K.J., Snyder, P.K., Foley, J.A., 2014. Drought and deforestation: has land cover change influenced recent precipitation extremes in the Amazon? J. Clim. 27 (1), 345–361. https://doi.org/10.1175/jcli-d-12-00369.1.

Bai, P., Liu, X.M., Zhang, Y.Q., Liu, C.M., 2018. Incorporating vegetation dynamics noticeably improved performance of hydrological model under vegetation greening. Sci. Total. Environ. 643, 610–622. https://doi.org/10.1016/j.scitotenv.2018.06.233.

Boone, A.A., et al., 2016. The regional impact of Land-Use Land-cover Change (LULCC) over West Africa from an ensemble of global climate models under the auspices of the WAMME2 project. Clim. Dynam. 47 (11), 3547–3573. https://doi.org/10.1007/s00382-016-3252-y.

Bounoua, L., DeFries, R., Collatz, G.J., Sellers, P., Khan, H., 2002. Effects of land cover conversion on surface climate. Clim. Change 52 (1–2), 29–64. https://doi.org/10.1023/A:1013051420309.

Brubaker, K.L., Entekhabi, D., Eagleson, P.S., 1993. Estimation of continental precipitation recycling. J. Clim. 6 (6), 1077–1089. https://doi.org/10.1175/1520-0442(1993)006<1077:EOCPR>2.0.CO;2.

Bryan, A.M., Steiner, A.L., Posselt, D.J., 2015. Regional modeling of surface-atmosphere interactions and their impact on Great Lakes hydroclimate. J. Geophys. Res.-Atmos. 120 (3), 1044–1064. https://doi.org/10.1002/2014JD022316.

Cao, Q., Yu, D.Y., Georgescu, M., Han, Z., Wu, J.G., 2015. Impacts of land use and land cover change on regional climate: a case study in the agro-pastoral transitional zone of China. Environ. Res. Lett. 10 (12), 124025. https://doi.org/10.1088/1748-9326/10/12/124025.

Chen, Y.H., Li, X.B., Su, W., Li, Y., 2008. Simulating the optimal land-use pattern in the farming-pastoral transitional zone of Northern China. Comput. Environ. Urban Syst. 32 (5), 407–414. https://doi.org/10.1016/j.compenvurbsys.2008.01.001.

Cheng, L., Zhang, L., Chiew, F.H.S., Canadell, J.G., Zhao, F.F., Wang, Y.P., Hu, X.Q., Lin, K.R., 2017. Quantifying the impacts of vegetation changes on catchment storage-discharge dynamics using paired-catchment data. Water Resour. Res. 53 (7), 5963–5979. https://doi.org/10.1002/2017WR020600.

Claussen, M., Brovkin, V., Ganopolski, A., 2001. Biogeophysical versus biogeochemical feedbacks of large-scale land cover change. Geophys. Res. Lett. 28 (6), 1011–1014. https://doi.org/10.1029/2000GL012471.

Cui, X.F., Graf, H.F., Langmann, B., Chen, W., Huang, R., 2006. Climate impacts of anthropogenic land use changes on the Tibetan Plateau. Global Planet. Change 54 (1–2), 33–56. https://doi.org/10.1016/j.gloplacha.2005.07.006.

Deng, Y., et al., 2018. Relationship among land surface temperature and LUCC, NDVI in typical karst area. Sci. Rep.-Uk 8 (1), 641. https://doi.org/10.1038/s41598-017-19088-x.

Dias, L.C.P., Macedo, M.N., Costa, M.H., Coe, M.T., Neill, C., 2015. Effects of land cover change on evapotranspiration and streamflow of small catchments in the Upper Xingu River Basin, Central Brazil. J. Hydrol: Regional Stud. 4, 108–122. https://doi.org/10.1016/j.ejrh.2015.05.010.

Dominguez, F., Kumar, P., Liang, X.Z., Ting, M.F., 2006. Impact of atmospheric moisture storage on precipitation recycling. J. Clim. 19 (8), 1513–1530. https://doi.org/10.1175/JCLI3691.1.

Eltahir, E.A.B., Bras, R.L., 2010. Precipitation recycling in the Amazon basin. Q. J. Roy. Meteor. Soc. 120 (518), 861–880. https://rmets.onlinelibrary.wiley.com/doi/pdf/10.1002/qj.49712051806.

Feng, X.M., Sun, G., Fu, B.J., Su, C.H., Lamparski, H., 2012. Regional effects of vegetation restoration on water yield across the Loess Plateau, China. Hydrol. Earth. Syst. Sci. 16 (8), 2617–2628. https://doi.org/10.5194/hess-16-2617-2012.

Foley, J.A., 2005. Global consequences of land use. Science 309 (5734), 570–574. https://doi.org/10.1126/science.1111772.

Fu, B.J., Liu, Y., Lü, Y.H., He, C.S., Zeng, Y., Wu, B.F., 2011. Assessing the soil erosion control service of ecosystems change in the Loess Plateau of China. Ecol. Complex. 8 (4), 284–293. https://doi.org/10.1016/j.ecocom.2011.07.003.

Gao, J.B., Wu, S.H., 2014. Simulated effects of land cover conversion on the surface energy budget in the southwest of China. Energies 7 (3), 1251–1264. https://doi.org/10.3390/en7031251.

Gao, Y., Leung, L.R., Zhao, C., Hagos, S., 2017. Sensitivity of U.S. summer precipitation to model resolution and convective parameterizations across gray zone resolutions. J. Geophys. Res.-Atmos. 122 (5), 2714–2733. https://doi.org/10.1002/2016JD025896.

Gleckler, P.J., Taylor, K.E., Doutriaux, C., 2008. Performance metrics for climate models. J. Geophys. Res.-Atmos. 113 (D6), D06104. https://doi.org/10.1029/2007JD008972.

Guo, L., Klingaman, N.P., Demory, M.E., Vidale, P.L., Turner, A.G., Stephan, C.C., 2018. The contributions of local and remote atmospheric moisture fluxes to East Asian precipitation and its variability. Clim. Dynam. 51 (11–12), 4139–4156. https://doi.org/10.1007/s00382-017-4064-4.

Guzha, A.C., Rufino, M.C., Okoth, S., Jacobs, S., Nobrega, R.L.B., 2018. Impacts of land use and land cover change on surface runoff, discharge and low flows: evidence from East Africa. J. Hydrol. 15, 49–67. https://doi.org/10.1016/j.ejrh.2017.11.005.

Hagos, S., et al., 2014. Assessment of uncertainties in the response of the African monsoon precipitation to land use change simulated by a regional model. Clim. Dynam. 43 (9–10), 2765–2775. https://doi.org/10.1007/s00382-014-2092-x.

Harding, R.J., Blyth, E.M., Tuinenburg, O.A., Wiltshire, A., 2013. Land atmosphere feedbacks and their role in the water resources of the Ganges basin. Sci. Total. Environ. 468, S85–S92. https://doi.org/10.1016/j.scitotenv.2013.03.016.

Hasler, N., Werth, D., Avissar, R., 2009. Effects of tropical deforestation on global hydroclimate: a multimodel ensemble analysis. J. Clim. 22 (5), 1124–1141. https://doi.org/10.1175/2008JCLI2157.1.

Hossain, F., Arnold, J., Beighley, E., et al., 2015. Local-to-regional landscape drivers of extreme weather and climate: implications for water infrastructure resilience. J. Hydrol. Eng. 20 (7), 02515002. https://doi.org/10.1061/(ASCE)HE.1943-5584.0001210.

Hu, H., Dominguez, F., 2015. Evaluation of oceanic and terrestrial sources of moisture for the North American monsoon using numerical models and precipitation stable isotopes. J. Hydrometeorol. 16 (1), 19–35. https://doi.org/10.1175/jhm-d-14-0073.1.

Hua, L.J., Zhong, L.H., Ke, Z.J., 2016. Precipitation recycling and soil-precipitation interaction across the arid and semi-arid regions of China. Int. J. Climatol. 36 (11), 3708–3722. https://doi.org/10.1002/joc.4586.

Huang, D., Wang, K., Wu, W., 2007. Problems and strategies for sustainable development of farming and animal husbandry in the Agro-Pastoral Transition Zone in Northern China (APTZNC). Int. J. Sustain. Dev. World. 14 (4), 391–399. https://doi.org/10.1080/13504500709469739.

Huang, H.Y., Margulis, S.A., 2010. Evaluation of a fully coupled large-eddy simulation-land surface model and its diagnosis of land-atmosphere feedbacks. Water Resour. Res. 46 (6), 666–669. https://doi.org/10.1029/2009WR008232.

Huang, H.Y., Margulis, S.A., 2011. Investigating the impact of soil moisture and atmospheric stability on cloud development and distribution using a coupled large-eddy simulation and land surface model. J. Hydrometeorol. 12 (5), 787–804. https://doi.org/10.1175/2011JHM1315.1.

Legesse, D., Vallet-Coulomb, C., Gasse, F., 2003. Hydrological response of a catchment to climate and land use changes in Tropical Africa: case study South Central Ethiopia. J. Hydrol. 275 (1–2), 67–85. https://doi.org/10.1016/S0022-1694(03)00019-2.

Lejeune, Q., Davin, E.L., Guillod, B.P., Seneviratne, S.I., 2014. Influence of Amazonian deforestation on the future evolution of regional surface fluxes, circulation, surface temperature and precipitation. Clim. Dynam. 44 (9–10), 2769–2786. https://doi.org/10.1007/s00382-014-2203-8.

Li, G., Zhang, F., Jing, Y., Liu, Y., Sun, G., 2017. Response of evapotranspiration to changes in land use and land cover and climate in China during 2001–2013. Sci. Total. Environ. 596–597, 256–265. https://doi.org/10.1016/j.scitotenv.2017.04.080.

Li, S., Sun, Z., Tan, M., Guo, L., Zhang, X., 2018. Changing patterns in farming–pastoral ecotones in China between 1990 and 2010. Ecol. Indic. 89, 110–117. https://doi.org/10.1016/j.ecolind.2018.01.067.

Li, S., An, P.L., Pan, Z.H., Li, X.M., Liu, Y., 2015. Farmers' initiative on adaptation to climate change in the Northern Agro-pastoral Ecotone. Int. J. Disast. Risk. Re. 12, 278–284. https://doi.org/10.1016/j.ijdrr.2015.02.002.

Li, X.Y., Hu, X., Zhang, Z.H., Peng, H.Y., Zhang, S.Y., Li, G.Y., Li, L., Ma, Y.J., 2013. Shrub hydropedology: preferential water availability to deep soil layer. Vadose Zone J. https://doi.org/10.2136/vzj2013.01.0006. doi: 10.2136/vzj2013.01.0006.

Li, Z., Chen, Y.N., Wang, Y., Fang, G.H., 2016. Dynamic changes in terrestrial net primary production and their effects on evapotranspiration. Hydrol. Earth Syst. Sci. 20 (6), 2169–2178. https://doi.org/10.5194/hess-20-2169-2016.

Liu, B., Zhao, W.Z., Wen, Z.J., Zhang, Z.H., 2014. Response of water and energy exchange to the environmental variable in a desert-oasis wetland of Northwest China. Hydrol. Process. 28 (25), 6098–6112. https://doi.org/10.1002/hyp.10098.

Liu, G., Zhang, Q., Li, G., Doronzo, D.M., 2016a. Response of land cover types to land surface temperature derived from Landsat-5 TM in Nanjing Metropolitan Region. China. Environ. Earth. Sci. 75 (20), 1386. https://doi.org/10.1007/s12665-016-6202-4.

Liu, J.H., Gao, J.X., Lv, S.H., Han, Y.W., Nie, Y.H., 2011. Shifting farming-pastoral ecotone in China under climate and land use changes. J. Arid. Environ. 75 (3), 298–308. https://doi.org/10.1016/j.jaridenv.2010.10.010.

Liu, M.X., Xu, X.L., Sun, A., 2015. Decreasing spatial variability in precipitation extremes in southwestern China and the local/large-scale influencing factors. J. Geophys. Res-Atmos. 120 (13), 6480–6488. https://doi.org/10.1002/2014JD022886.

Liu, Z.P., Wang, Y.Q., Shao, M.A., Jia, X.X., Li, X.L., 2016b. Spatiotemporal analysis of multiscalar drought characteristics across the Loess Plateau of China. J. Hydrol. 534, 281–299. https://doi.org/10.1016/j.jhydrol.2016.01.003.

Mahmood, R., et al., 2010. Impacts of land use/land cover change on climate and future research priorities. B. Am. Meteorol. Soc. 91 (1), 37–46. https://doi.org/10.1175/2009BAMS2769.1.

Mao, D., Cherkauer, K.A., 2009. Impacts of land-use change on hydrologic responses in the Great Lakes region. J. Hydrol. 374 (1–2), 71–82. https://doi.org/10.1016/j.jhydrol.2009.06.016.

Mohan, M., Kandya, A., 2015. Impact of urbanization and land-use/land-cover change on diurnal temperature range: a case study of tropical urban airshed of India using remote sensing data. Sci. Total. Environ. 506–507, 453–465. https://doi.org/10.1016/j.scitotenv.2014.11.006.

Mahmood, R., Pielke Sr, R.A., Hubbard, K.G., et al., 2014. Land cover changes and their biogeophysical effects on climate. Int. J. Climatol. 34 (4), 929–953. https://doi.org/10.1002/joc.3736.

Moriasi, D.N., Arnold, J.G., Van Liew, M.W., Bingner, R.L., Harmel, R.D., Veith, T.L., 2007. Model evaluation guidelines for systematic quantification of accuracy in watershed simulations. T. ASABE 50 (3), 885–900. https://doi.org/10.13031/2013.23153.

Olchev, A., Ibrom, A., Priess, J., Erasmi, S., Leemhuis, C., Twele, A., Radler, K., Kreilein, H., Panferov, O., Gravenhorst, G., 2008. Effects of land-use changes on evapotranspiration of tropical rain forest margin area in Central Sulawesi (Indonesia): Modelling study with a regional SVAT model. Ecol. Model. 212 (1), 131–137. https://doi.org/10.1016/j.ecolmodel.2007.10.022.

Orlowsky, B., Seneviratne, S.I., 2010. Statistical analyses of land–atmosphere feedbacks and their possible pitfalls. J. Clim. 23 (14), 3918–3932. https://doi.org/10.1175/2010JCLI3366.1.

Pielke, R.A., Andy, P., Dev, N., Rezaul, M., et al., 2011. Land use/land cover changes and climate: modeling analysis and observational evidence. Wires. Clim. Change 2 (6), 828–850. https://doi.org/10.1002/wcc.144.

Pielke, R.A., Mahmood, R., McAlpine, C., 2016. Land's complex role in climate change. Phys. Today 69 (2016), 40–46. https://doi.org/10.1063/PT.3.3364.

Pitman, A.J., Noblet-Ducoudré, N., Cruz, F.T., Davin, E.L., et al., 2009. Uncertainties in climate responses to past land cover change: first results from the LUCID intercomparison study. Geophys. Res. Lett. 36 (14). https://doi.org/10.1029/2009GL039076.

Qiao, L., Zou, C.B., Stebler, E., Will, R.E., 2017. Woody plant encroachment reduces annual runoff and shifts runoff mechanisms in the tallgrass prairie, USA. Water

Resour. Res. 53 (6), 4838–4849. https://doi.org/10.1002/2016WR019951.
Qin, P.H., Xie, Z.H., 2017. Precipitation extremes in the dry and wet regions of China and their connections with the sea surface temperature in the eastern tropical Pacific Ocean. J. Geophys. Res-Atmos. 122 (12), 6273–6283. https://doi.org/10.1002/2016JD026242.
Qu, R.J., Cui, X.L., Yan, H.M., Ma, E.J., Zhan, J.Y., 2013. Impacts of land cover change on the near-surface temperature in the North China Plain. Adv. Meteorol. 2013, 1–12. https://doi.org/10.1155/2013/409302.
Rajeevan, M., Kesarkar, A., Thampi, S.B., Rao, T.N., Radhakrishna, B., Rajasekhar, M., 2010. Sensitivity of WRF cloud microphysics to simulations of a severe thunderstorm event over Southeast India. Ann. Geophys. 28 (2), 603–619. https://doi.org/10.5194/angeo-28-603-2010.
Rigden, A.J., Li, D., 2017. Attribution of surface temperature anomalies induced by land use and land cover changes. Geophys. Res. Lett. 44 (13), 6814–6822. https://doi.org/10.1002/2017GL073811.
Roy, S.B., Avissar, R., 2002. Impact of land use/land cover change on regional hydrometeorology in Amazonia. 107(D20): LBA-1-LBA. J. Geophys. Res-Atmos. 4–12. https://doi.org/10.1029/2000JD000266.
Sen, O.L., Wang, Y., Wang, B., 2004. Impact of Indochina deforestation on the East Asian summer monsoon. J. Clim. 17 (6), 1366–1380. https://doi.org/10.1175/1520-0442(2004) 017<1366:IOIDOT>2.0.CO;2.
Silverman, N.L., Maneta, M.P., Chen, S.H., Harper, J.T., 2013. Dynamically downscaled winter precipitation over complex terrain of the Central Rockies of Western Montana, USA. Water Resour. Res. 49 (1), 458–470. https://doi.org/10.1029/2012WR012874.
Skamarock, W.C., Klemp, J.B., Dudhia, J., Gill, D.O., Barker, D.M., Duda, M.G., Huang, X. Y., Wang, W., Powers, J.G., 2008. A description of the advanced research WRF version 3, NCAR Technical Note. National Center for Atmospheric Research: Boulder, CO, USA, 2008. http://www2.mmm.ucar.edu/wrf/users/docs/arw_v3_bw.pdf.
Snyder, P.K., 2010. The influence of tropical deforestation on the northern hemisphere climate by atmospheric teleconnections. Earth Interact. 14 (4), 1–34. https://doi.org/10.1175/2010EI280.1.
Snyder, P.K., Delire, A.C., Foley, J.A., 2004. Evaluating the influence of different vegetation biomes on the global climate. Clim. Dynam. 23, 279–302. https://doi.org/10.1007/s00382-004-0430-0.
Sohrabinia, M., Rack, W., Zawar-Reza, P., 2012. Analysis of MODIS LST compared with WRF model and in situ data over the Waimakariri River Basin, Canterbury, New Zealand. Remote. Sens.-Basel. 4 (11), 3501–3527. https://doi.org/10.3390/rs4113501.
Teixeira, J.C., Carvalho, A.C., Carvalho, M.J., Luna, T., Rocha, A., 2014. Sensitivity of the WRF model to the lower boundary in an extreme precipitation event–Madeira island case study. Nat. Hazard. Earth. Syst. Sci. 14 (8), 2009–2025. https://doi.org/10.5194/nhess-14-2009-2014.
Taylor, K.E., 2001. Summarizing multiple aspects of model performance in a single diagram. J. Geophys. Res.-Atmos. 106 (D7), 7183–7192. https://doi.org/10.1029/2000JD900719.
Wagner, S., Fersch, B., Yuan, F., Yu, Z.B., Kunstmann, H., 2016. Fully coupled atmospheric-hydrological modeling at regional and long-term scales: development, application, and analysis of WRF-HMS. Water Resour. Res. 52 (4), 3187–3211. https://doi.org/10.1002/2015WR018185.
Wan, Q.L., Xu, J.J., 2011. A numerical study of the rainstorm characteristics of the June 2005 flash flood with WRF/GSI data assimilation system over south-east China. Hydrol. Process. 25 (8), 1327–1341. https://doi.org/10.1002/hyp.7882.
Wang, C., Gao, Q., Wang, X., Yu, M., 2015a. Decadal trend in agricultural abandonment and wwoodland expansion in an Agro-Pastoral Transition Band in Northern China. PloS One 10 (11), e0142113. https://doi.org/10.1371/journal.pone.0142113.
Wang, K., Zhang, Q., Chen, Y.D., Singh, V.P., 2015b. Effects of land-use/cover change on hydrological processes using a GIS/RS-based integrated hydrological model: case study of the East River, China. Hydrol. Sci. J. 60 (10), 1724–1738. https://doi.org/10.1080/02626667.2014.949723.
Wang, S., Zhang, M., Che, Y., Chen, F., Qiang, F., 2016. Contribution of recycled moisture to precipitation in oases of arid central Asia: a stable isotope approach. Water Resour. Res. 52 (4), 3246–3257. https://doi.org/10.1002/2015WR018135.
Wei, B.C., Xie, Y.W., Jia, X., Wang, X.Y., He, H.J., Xue, X.Y., 2018. Land use/land cover change and it's impacts on diurnal temperature range over the agricultural pastoral ecotone of Northern China. Land Degrad. Dev. 29 (9), 3009–3020. https://doi.org/10.1002/ldr.3052.
Wei, J., Dirmeyer, P.A., Bosilovich, M.G., Wu, R., 2012. Water vapor sources for Yangtze River valley rainfall: climatology, variability, and implications for rainfall forecasting. J. Geophys. Res.-Atmos. 117, D05126. https://doi.org/10.1029/2011JD016902.
Wei, J.F., Su, H., Yang, Z.L., 2016. Impact of moisture flux convergence and soil moisture on precipitation: a case study for the southern United States with implications for the globe. Clim. Dynam. 46 (1–2), 467–481. https://doi.org/10.1007/s00382-015-2593-2.
Wen, X.H., Lu, S.H., Jin, J.M., 2012. Integrating remote sensing data with WRF for improved simulations of oasis effects on local weather processes over an arid region in northwestern China. J. Hydrometeorol. 13 (2), 573–587. https://doi.org/10.1175/Jhm-D-10-05001.1.
Wijesekara, G.N., Gupta, A., Valeo, C., Hasbani, J.G., Qiao, Y., Delaney, P., Marceau, D.J., 2012. Assessing the impact of future land-use changes on hydrological processes in the Elbow River watershed in southern Alberta, Canada. J. Hydrol. 412, 220–232. https://doi.org/10.1016/j.jhydrol.2011.04.018.
Woodward, C., Shulmeister, J., Larsen, J., Jacobsen, G.E., Zawadzki, A., 2014. The hydrological legacy of deforestation on global wetlands. Science 346 (6211), 844–847. https://doi.org/10.1126/science.1260510.
Wu, F., Zhan, J.Y., Yan, H.M., Shi, C.C., Huang, J., 2013a. Land cover mapping based on multisource spatial data mining approach for climate simulation: a case study in the Farming-Pastoral Ecotone of North China. Adv. Meteorol. 2013, 520803. https://doi.org/10.1155/2013/520803.
Wu, Z.T., Wu, J.J., Liu, J.H., He, B., Lei, T.J., Wang, Q.F., 2013b. Increasing terrestrial vegetation activity of ecological restoration program in the Beijing-Tianjin Sand Source Region of China. Ecol. Eng. 52, 37–50. https://doi.org/10.1016/j.ecoleng.2012.12.040.
Xia, Y.L., Hao, Z.C., Shi, C.X., Li, Y.H., et al., 2019. Regional and global land data assimilation systems: innovations, challenges, and prospects. J. Meteorol. Res. 33 (2), 159–189. https://doi.org/10.1007/s13351-019-8172-4.
Xia, Y.L., Mocko, D., Huang, M.Y., Li, B.L., Rodell, M.E., Mitchell, K.E., Cai, X.T., Ek, M.B., 2017. Comparison and assessment of three advanced land surface models in simulating terrestrial water storage components over the United States. J. Hydrometeorol. 18 (3), 625–649. https://doi.org/10.1175/JHM-D-16-0112.1.
Xue, Y.K., et al., 2010. Intercomparison and analyses of the climatology of the West African Monsoon in the West African Monsoon Modeling and Evaluation project (WAMME) first model intercomparison experiment. Clim. Dynam. 35 (1), 3–27. https://doi.org/10.1007/s00382-010-0778-2.
Yuan, G.H., et al., 2017. Impacts of initial soil moisture and vegetation on the diurnal temperature range in arid and semiarid regions in China. J. Geophys. Res.-Atmos. 122 (21), 11568–11583. https://doi.org/10.1002/2017JD026790.
Zabel, F., Mauser, W., Marke, T., Pfeiffer, A., Zangl, G., Wastl, C., 2011. Inter-comparison of two land-surface schemes applied on different scales and their feedbacks while coupled with a regional climate model. Hydrol. Earth Syst. Sci. Discuss. 8 (4), 7091–7136. https://doi.org/10.5194/hessd-8-7091-2011.
Zhang, B.Q., Wu, P.T., Zhao, X.N., Wang, Y.B., Wang, J.W., Shi, Y.J., 2012a. Drought variation trends in different subregions of the Chinese Loess Plateau over the past four decades. Agric. Water. Manage. 115, 167–177. https://doi.org/10.1016/j.agwat.2012.09.004.
Zhang, C., Tang, Q., Chen, D., 2017. Recent changes in the moisture source of precipitation over the Tibetan Plateau. J. Clim. 30 (5), 1807–1819. https://doi.org/10.1175/jcli-d-15-0842.1.
Zhang, S.L., Yang, D.W., Jayawardena, A.W., Xu, X.Y., Yang, H.B., 2016a. Hydrological change driven by human activities and climate variation and its spatial variability in Huaihe Basin, China. Hydrol. Sci. J. 61 (8), 1370–1382. https://doi.org/10.1080/02626667.2015.1035657.
Zhang, S.L., Yang, H., Yang, D.W., et al., 2016b. Quantifying the effect of vegetation change on the regional water balance within the Budyko framework. Geophys. Res. Lett. 43 (3), 1140–1148. https://doi.org/10.1002/2015GL066952.
Zhang, X., Tang, Q., Zheng, J., Ge, Q., 2013. Warming/cooling effects of cropland greenness changes during 1982–2006 in the North China Plain. Environ. Res. Lett. 8 (2), 024038. https://doi.org/10.1088/1748-9326/8/2/024038.
Zhang, X., et al., 2015. Using multi-model ensembles to improve the simulated effects of land use/cover change on temperature: a case study over northeast China. Clim. Dynam. 46 (3–4), 765–778. https://doi.org/10.1007/s00382-015-2611-4.
Zhang, Y.F., Guan, D.X., Jin, C.J., Wang, A.Z., Wu, J.B., Yuan, F.H., 2014. Impacts of climate change and land use change on runoff of forest catchment in northeast China. Hydrol. Process. 28 (2), 186–196. https://doi.org/10.1002/hyp.9564.
Zhang, Y., Liang, S., 2018. Impacts of land cover transitions on surface temperature in China based on satellite observations. Environ. Res. Lett. 13 (2), 024010. https://doi.org/10.1088/1748-9326/aa9e93.
Zhang, Z.X., Xu, C.Y., Yong, B., Hu, J.J., Sun, Z.H., 2012b. Understanding the changing characteristics of droughts in Sudan and the corresponding components of the hydrologic cycle. J. Hydrometeorol. 13 (12), 1520–1535. https://doi.org/10.1175/JHM-D-11-0109.1.
Zhao, L., Liu, Y., Pan, Z., An, P.L., Pan, X.B., Zhao, P.Y., 2013. Impacts of recent climate change on dry-land crop water consumption in the northern agro-pastoral transitional zone of China. Acta Meteorol. Sin. 27 (4), 585–590. https://doi.org/10.1007/s13351-013-0405-3.
Zhao, T., Zhao, J., Hu, H., Ni, G., 2016. Source of atmospheric moisture and precipitation over China's major river basins. Front. Earth. Sci.-Process 10 (1), 159–170. https://doi.org/10.1007/s11707-015-0497-4.
Zhao, W., Hu, Z.M., Li, S.H., Guo, Q., Liu, Z.J., Zhang, L.M., 2017. Comparison of surface energy budgets and feedbacks to microclimate among different land use types in an agro-pastoral ecotone of northern China. Sci. Total Environ. 599, 891–898. https://doi.org/10.1016/j.scitotenv.2017.04.200.
Zhao, X.S., Huang, Y., Jia, Z.J., Liu, H.Z., Song, T., et al., 2008. Effects of the conversion of marshland to cropland on water and energy exchanges in northeastern China. J. Hydrol. 355 (1–4), 181–191. https://doi.org/10.1016/j.jhydrol.2008.03.019.
Zhou, L.H., Zhu, Y.L., Yang, G.J., Luo, Y.Q., 2013. Quantitative evaluation of the effect of prohibiting grazing policy on grassland desertification reversal in northern China. Environ. Earth. Sci. 68 (8), 2181–2188. https://doi.org/10.1007/s12665-012-1901-y.